

Functional linkage between TRPV4 and calcium-activated
chloride channels in choroid plexus epithelial cells

Yasunori Takayama

Doctor of Philosophy
(Science)

Department of Physiological Science,
School of Life Science,
The Graduate University for Advanced Studies

2013

Index

1. Abstract	3
2. Introduction	6
3. Materials and Methods	9
4. Result	15
Expression pattern of <i>Trpv4</i>	
Functional expression of TRPV4 in CPECs	
Currents of calcium-activated chloride channels in CPECs	
Expression pattern of <i>Ano1</i> in CPECs	
Current properties of ANO1-mediated currents	
Functional linkage between TRPV4 and ANO1	
Heat-evoked chloride currents in CPECs	
5. Discussion	21
6. Acknowledgements	25
7. References	27
8. Tables	33
9. Fiure Legends	35
10. Figres	42

1. Abstract

Transient receptor potential vanilloid 4 (TRPV4) is a non-selective cation channel known to be a sensor for hypo-osmolality, cell swelling, warm temperatures and some chemical compounds. Furthermore, the physiological significance of TRPV4 has attracted a great deal of attention, particularly its heat-sensitive properties. Previous reports showed the physiological functions of TRPV4 in several cell types, including skin, esophageal keratinocytes and hippocampal neurons. For instance, TRPV4 expressed in skin keratinocytes contributes to the enhancement of the skin barrier function at body temperature. Moreover, the release of ATP from esophageal keratinocytes or bladder epithelium is enhanced by extension-mediated TRPV4 activation. Additionally, neural activity increases with a rise in temperature in hippocampal neurons. However, the precise function of TRPV4 in the brain is still unknown except for regulation of neural activity in the hippocampus. In this study, the highest expression of TRPV4 in choroid plexus epithelial cells (CPECs) was found using *in situ* hybridization, immunohistochemistry and EGFP expression in transgenic mice in which EGFP was expressed in TRPV4-positive cells. In addition, calcium-activated chloride currents were observed for the first time in CPECs. Moreover, expression of anoctamin 1 (*Ano1*), *Ano4*, *Ano6* and *Ano10* genes in the choroid plexus was found by RT-PCR. These data suggest that upon TRPV4 activation, calcium entering CPECs enhances production of cerebrospinal fluid (CSF), a process dependent upon ion transports. To investigate this hypothesis, whole-cell patch-clamp recordings in HEK293T cells were performed. ANO1-mediated chloride currents were dramatically increased in HEK293T cells expressing mouse TRPV4 and mouse ANO1 when TRPV4 was activated by a low concentration of GSK1016790A (GSK). In contrast, the GSK-induced chloride currents were not significantly affected in the cells expressing ANO4, ANO6 or ANO10 with TRPV4. Additionally, the GSK-induced chloride currents

in the cells expressing ANO1 and TRPV4 were not observed in the absence of extracellular calcium. These results indicated that chloride efflux through ANO1 depended on TRPV4 activity. Similar GSK-induced chloride currents were observed in CPECs isolated from the lateral and the fourth ventricle choroid plexus. Interestingly, the GSK-induced chloride currents were strongly inhibited by an ANO1/ANO2 blocker, T16Ainh-A01 (A01), and ANO2 expression was not suggested in choroid plexus. These results indicated a functional linkage between TRPV4 and ANO1 in CPECs. This is the first reported case of the linkage of these two proteins in native cells. It was recently reported that ANO1 is activated by noxious heat. In the author's study, ANO1 was activated by heat in the range of body temperature. Heat-evoked chloride currents were also observed in CPECs isolated from wild-type (WT) and TRPV4-deficient (TRPV4KO) mice. Furthermore, heat-evoked currents were drastically enhanced after GSK application in WT, but not in TRPV4KO CPECs. These results indicated the possibility that heat-sensitivity of ANO1 is enhanced by TRPV4 activation in CPECs. However, the enhanced currents were not completely blocked by A01. Thus, the possibility of another heat-activated chloride channels also was suggested in CPECs.

Accordingly, the author proposes a concept that functional linkage between TRPV4 and ANO1 enhances CSF production. First, the apical membrane of CPECs is extended by water influx from the basolateral side. Second, phospholipase A₂ (PLA₂) activity is increased by the extension of the plasma membrane and arachidonic acid is produced from phospholipids by the activated PLA₂. Then, arachidonic acid is metabolized to epoxyeicosatrienoic acid (EET) by cytochrome P450 epoxygenase activity, and TRPV4 is activated by EET at body temperature. The TRPV4 activation leads to calcium influx, which in turn leads to ANO1 activation at body temperature. Finally, water efflux from CPECs is driven by efflux of chloride and some cations through a Donnan equilibrium. Production, transport

and reabsorption of CSF are important for the maintenance of the brain environment in fetuses and adults. Among the three CSF-related events, the principle role of CPECs is CSF production. CSF transport is controlled by ependymal cells and the reabsorption is done by arachnoid granulation to the dural venous sinuses. Dysfunction of ciliary motility and the failure of cilia development of ependymal cells induce severe hydrocephalus. This indicates that CSF is continuously secreted from CPECs and the production is independent of the changes in brain pressure. There are currently only palliative therapies for hydrocephalus including external ventricular drainage or placement of a surgical shunt. Control of CSF production through regulation of TRPV4 activity could allow a safer way to treat those diseases. Thus, these studies suggest a fundamental new therapy for hydrocephalus caused by choroid plexus cysts and choroid plexus papillomas.

2. Introduction

Transient receptor potential (TRP) channels are categorized as non-selective cation channels. The TRP channel superfamily includes a group of thermo-sensitive channels ; TRPV1, TRPV2, TRPV3, TRPV4, TRPM2, TRPM4, TRPM5, TRPM8 and TRPA1¹⁻⁹. Although TRPV1, TRPV2, TRPM8 and TRPA1 are activated by the dynamic changes of ambient temperature against body temperature, temperature thresholds for the activation of TRPV3, TRPV4, TRPM2, TRPM4 and TRPM5 are in the warm temperature range. TRPV4 was originally reported to be an osmo- or mechano-sensor^{10,11} that was activated by diverse chemical stimuli, including synthetic phorbol ester 4 α -phorbol 12, 13-didecanoate (4 α -PDD)¹² and GSK1016790A¹³ as well as moderate warmth (>27°C)^{4,5}. Furthermore, an endogenous agonist for TRPV4, epoxyeicosatrienoic acid (EET), is produced in the arachidonic acid cascade occurred by PLA₂ activity via plasma membrane extension¹⁴. There are 4 types of EET, including 5'6'-EET, 8'9'-EET, 11'12'-EET and 14'15'-EET. Although 5'6'-EET and 8'9'-EET are effective compounds, 11'12'-EET and 14'15'-EET are ineffective¹⁴. Therefore, TRPV4 could play important roles involving calcium and EETs in tissues that are influenced by body temperature. Previous reports showed the physiological significances of TRPV4 in several cell types, including skin, bladder epithelium, esophageal keratinocytes and hippocampal neurons. For instance, an adherens junction is reinforced by means of TRPV4 activity in skin keratinocytes¹⁵. In addition, TRPV4 activation enhances release of ATP from bladder epithelium and esophageal keratinocytes^{16,17}. Moreover, firing rates increase upon depolarization via TRPV4 activation at body temperature in hippocampal neurons¹⁸. Nevertheless, the physiological significance of TRPV4 in the choroid plexus is unknown. Therefore, the focus of the author's work was the function of TRPV4 in the choroid plexus.

The choroid plexus is involved in the maintenance of the brain environment in the lateral, the third and the fourth ventricles. These tissues form a continuous monolayer structure with epithelial cells, leptomeninges and fenestrated capillaries¹⁹. Choroid plexus epithelial cells (CPECs) are separated into apical and basolateral membrane by tight junctions between CPECs (Fig. 2a). The apical membrane faces the CSF in the ventricles while the basolateral membrane is on the side of fenestrated capillaries. This structure is very important for the formation of the blood-CSF barrier. Another function of CPECs is absorption of the metabolites of neurotransmitters such as serotonin and dopamine²⁰. The most important function of CPECs is CSF production. CSF production depends on electrolyte transports from basolateral to apical membrane of CPECs²¹. Sodium is transported to CPECs by Na/HCO₃ co-transporters in the basolateral membrane²². At the same time, bicarbonate is transported to CPECs by Na/HCO₃ co-transporters. And it is thought that sodium is released to the ventricle through the apical membrane by a Na/K ATPase²³ and Na/K/Cl co-transporters²⁴. Then, potassium also is released to the ventricle by Na/K/Cl co-transporters and K/Cl co-transporters²⁵. Meanwhile, chloride is also transported to CPECs by Cl/HCO₃ exchangers²⁶, and chloride is released by Na/K/Cl co-transporters, chloride channels and K/Cl co-transporters. These ion transports induce water flux from the basolateral to the apical membrane through aquaporin 1²⁷. Thus, CSF is produced in CPECs by ion transports.

CSF secreted by CPECs is moved through the ventricles by cilia-coated ependymal cells that cover the surfaces of the ventricles²⁸. Tufts of cilia appear around five days after birth, and gradually increase to their mature density over five days²⁹. The motile cilia make a CSF flow, and the mean flow velocity is approximately 100 - 200 $\mu\text{m}/\text{sec}$ with a maximum speed of 400 $\mu\text{m}/\text{sec}$ as determined in the author's experiments using 15 μm diameter fluorescent beads (Fig S1). Although the flow is

complex in various parts of the ventricles³⁰, circulation is roughly from the third ventricle to the subarachnoid space. Most of the CSF moved to the subarachnoid space via the foramen of Lushuka or Magendie in the fourth ventricle. Reabsorption of CSF from arachnoid granulation to dural venous sinuses is enhanced by an increase of CSF pressure over 70 mm H₂O³¹. This circulation is important to develop central nervous system and to maintain the brain environment because severe hydrocephalus is caused by failure of motile ciliary morphogenesis, and the waste substances from neurons or glial cells are delivered by the CSF flow. Therefore, production, transport and reabsorption of CSF are essential for vertebrates.

Recently, it was reported that the high calcium permeability of TRPV4 activated some calcium-activated channels, such as a small conductance calcium-activated potassium channel and an intermediate conductance calcium-activated potassium channel³². The author discovered the functional expression of calcium-activated chloride channels in isolated CPECs of mice. Here, it was hypothesized that TRPV4 might affect CSF production through interaction with calcium-activated chloride channels because the equilibrium potential for chloride in CPECs is approximately -20 mV^{19,33}, leading to chloride efflux upon chloride channel activation. Thus, the author investigated the physiological interaction of TRPV4 with calcium-activated chloride channels in the CPECs of mice.

3. Materials and Methods

Mice

All mouse experiments were conducted with four- to ten-week-old C57BL/6NCr mice. TRPV4-deficient (TRPV4KO) and transgenic mice were backcrossed on a C57BL/6NCr background. All animal experimental procedures were performed according to the National Institute for Physiological Sciences guidelines.

Chemicals

5-nitro-2-(3-phenylpropylamino) benzoic acid (NPPB), ionomycin calcium salt, GSK1016790A and adenosine 5'-triphosphate (ATP) disodium salt were purchased from Sigma. T16Ainh-A01 was purchased from CALBIOCHEM. HC067047 was purchased from TOCRIS. Serotonin, norepinephrine and bradykinin were purchased from the Peptide Institute.

Generation of transgenic mice

Bacterial artificial chromosome (BAC) transgenic mice which express EGFP specifically in TRPV4-positive cells were generated by Research Institute for Microbial Diseases, Osaka University. TRE-EGFP-2A-mtTA-c-Myc DNA fragment (3 kb) was synthesized by Biomatik Co. (United States), was inserted into a pPE7neoW_F2LF plasmid which inserted 5' and 3' homology arms (~400 bp). The homologous arms were obtained by PCR with PrimeStar (TAKARA, Japan). The 5'-homologous region primer sets were as follows: 5'-ACT TAA GGG GGC ACT TGT AGG CAT TCT G-3' and 5'-AGC TAG CAC TGG ACC CAG ATC TGT TTG TAC-3'. The 3'-homologous region primer sets were as follows: 5'-TAA GCT TTG GAC GTC CAA ACC TGC GTA TGA AG-3' and 5'-TCT

CGA GGA TGG ATG GAT GGA TGG ATA G-3'. TRE-EGFP-2A-mtTA-c-Myc DNA fragment with 5' and 3' homology arms was excised from plasmid and introduced in E. Coli carried BAC (RP23-328P23) by electroporation. BAC clone, which inserted DNA fragment containing TRE-EGFP-2A-mtTA-c-Myc DNA in TRPV4 allele was selected as neomycin resistance. BAC was extracted and purified by NucleoBond BAC 100 (Macherey-nagel, Germany). BAC DNA was dissolved in an injection buffer and microinjected into pronuclei of fertilized mouse eggs (C57BL/6 mice) to generate transgenic founders. Primer sets for EGFP genotyping were as follows 5'-CAC AAG TTC AGC GTG TCC G-3' and 5'-GTG AAC CGC ATC GAG CTG A-3'.

RT-PCR

Total RNA was purified from the choroid plexus of WT or TRPV4KO mice using Sepasol-RNA I super G (Nacalai Tesque, Japan). Reverse transcription with a cDNA library was performed using Super Script III reverse transcriptase (Invitrogen, United States) for one hr at 55°C. For investigation of anoctamin mRNA expression patterns in the choroid plexus, DNA fragments were amplified using EmeraldAmp PCR Master Mix (TAKARA, Japan) with PCR primers designed using pick primers from the National Center for Biotechnology Information (Table. S1). The PCR products were confirmed by electrophoresis on 1 % agarose gel containing ethidium bromide.

Histological analysis

C57BL/6Ncr, TRPV4KO and transgenic mice were anaesthetized with isoflurane and perfused with 20 mL of ice-cold PBS containing 137 mM NaCl, 2.68 mM KCl, 8.10 mM Na₂HPO₄, 1.47 mM KH₂PO₄, and 20 mL of ice-cold fixative solution consisting of 4% paraformaldehyde in 0.1 M PBS. The fixed

brain was removed into the fixative solution and immersed for 16 hr at 4°C. The brains were subsequently immersed twice in 30% sucrose in PBS for 24 hr at 4°C. The brains were embedded in OCT compound and sectioned at 40 µm thickness for immunohistochemistry. To perform immunohistochemistry, the sections were blocked in PBS containing 0.25% Triton X and 1% bovine serum albumin for 30 min at room temperature. Sections were then incubated with rabbit anti-TRPV4 antibody (1:1000, a generous gift from Professor B. Nilius), rabbit anti-GFP antiserum (1:1000, Molecular Probes, United States), rabbit anti-ANO1 antibody (1:300, a generous gift from Professor U. Oh), and mouse anti-NaK ATPase α 1 ascites fluid (1:300, a generous gift from Assistant Professor A. Imura) for 16 hr at 4°C. The sections were reacted with Alexa 488, Alexa 594 or Alexa 633 (Molecular Probes, United States) for one hr at room temperature. For immunostaining of isolated CPECs, the cells were immersed in the fixative solution for ten min at room temperature, and immersed twice in 30% sucrose PBS for 24 hr at 4°C. The cells were blocked for 30 min at room temperature and incubated with mouse anti-NaK ATPase α 1 ascites fluid (1:300) diluted in blocking solution for 16 hr at 4°C and then reacted with Alexa 594 for 1 hr at room temperature and DAPI for 3 min at room temperature. These stained samples were mounted and examined with a fluorescence microscope or a confocal microscope.

Isolation of CPECs

The choroid plexus was separated from the lateral and the fourth ventricles of each mouse which were anesthetized by isoflurane. These anesthetized mice were perfused with 10 mL ice-cold artificial cerebrospinal fluid (aCSF) consisting of the following: 124 mM NaCl, 5 mM KCl, 1.2 mM KH₂PO₄, 1.3 mM MgSO₄, 2.4 mM CaCl₂, 10 mM glucose, 24 mM NaHCO₃ and bubbled with 95% O₂ and 5%

CO₂ for at least 1 hr on ice, from left chamber of the heart, and incubated with the ice-cold aCSF. After 20 min, the tissues were washed twice with calcium- and magnesium-free PBS (-) (Wako, Japan). The tissues were incubated with 250 µg collagenase type IX (Sigma, United States) in 100 µL PBS (-) for 15 min at 37°C. The tissues were then incubated with the same enzyme solution a second time for 10 min at 37°C after gently dissociating with a larger diameter Pasteur pipette. Next, the clusters of CPECs were isolated with a small diameter Pasteur pipette. After that, CPECs were isolated with a small pipette, and 900 µL PBS (-) was added. The isolated cells were centrifuged (300 × g) for 10 min at 4°C. The pellets were suspended in 1 mL of fresh PBS (-). After the second centrifugation, the isolated cells were placed on 1 cm diameter cover slips (Matsunami, Japan) with 40 µL each of high glucose D-MEM with L-glutamine and phenol red (Wako, Japan) containing 10% inactivated fetal bovine serum (lot# S06537S1560, Biowest, France), 50 units penicillin / 50 µg streptomycin (Gibco, United States) and GlutaMAX (Gibco, United States). All experiments with isolated CPECs were performed after incubating the cells for 1 hr at 33°C in a 5% CO₂ humidified incubator. The CPECs were used within 6 hr of isolation.

Patch-clamp recording

Patch pipettes were made from borosilicate glass (type 8250, Garner Glass Company, United States) with a five-step protocol in P-2000 (Sutter Instrument, United States), and the tip resistance was 4 to 6 MΩ. Currents were recorded using an Axopatch 200B amplifier (Molecular Devices, United States) and filtered at 5 kHz with a low-pass filter. Currents were digitized with Digidata 1440A (Axon Instruments, United States). Data acquisition software, pCLAMP 10 (Axon Instruments, United States), was used. The standard bath solution contained 130 mM NaCl, 5 mM KCl, 1 mM MgCl₂, 2

mM CaCl₂, 10 mM glucose, 10 mM HEPES, pH 7.40 with NaOH. The standard pipette solution contained 140 mM KCl, 1 mM MgCl₂, 5 mM EGTA, 10 mM HEPES, pH 7.30 with KOH. The NMDG-Cl bath solution contained 135 mM NMDG-Cl, 1 mM MgCl₂, 2 mM CaCl₂, 10 mM glucose, 10 mM HEPES, pH 7.40 with NMDG. The NMDG-Cl pipette solution for HEK293T cells contained 140 mM NMDG-Cl, 1 mM MgCl₂, 5 mM BAPTA, 10 mM HEPES, pH 7.30 with NMDG. The NMDG-Cl pipette solution for CPECs contained 140 mM NMDG-Cl, 1 mM MgCl₂, 0.2 mM EGTA, 10 mM HEPES, pH 7.30 with NMDG. The intracellular free calcium concentration was calculated with the MAXC program of Stanford University. Mouse TRPV4 and/or mouse ANO1, ANO4, ANO6 or ANO10 plasmids (a generous gift from Professor U. Oh) (1 µg each) were transfected into HEK293T cells with 0.1 µg pGreen Lantern-1 plasmid and incubated for at least 24 hr at 33°C in a 5% CO₂ humidified incubator. Thermal stimulation was applied by increasing the bath temperature with preheated solution in water bath. All data and graphs were statistically analyzed using Origin Pro 8 (OriginLab, United States).

Immunoprecipitation and Western Blot

All proteins were extracted from HEK293T cells incubated for 24 hr in the 5% CO₂ humidified incubator at 33°C after transfection. The cells were washed with PBS. Samples were centrifuged for 5 min at 300 × g. The pellets were resuspended in lysis buffer with 1% Nonidet P-40 contained 150 mM NaCl, 20 mM HEPES, 1 mM EDTA, for 30 min. Following centrifugation at 161,000 × g for 30 min, the supernatants were incubated in a rotator for 2 hr with protein G (GE Healthcare, United States). Following centrifugation at 2,000 × g for 5 min, the supernatants were incubated in a rotator for 16 hr with two µg anti-TRPV4 antibody (abcam; ab39260, United States) or the anti-ANO1 antibody. After

incubation, protein G binding with magnetic beads (GE Healthcare) was added, and the solutions were incubated in rotator for 2 hr. After incubation, these magnetic beads were washed by lysis buffer, and the proteins were denated by SDS buffer contained 0.5 M Tris-HCL, 10% sodium dodecylsulphate, 6% b-mercaptoethanol, 10% glycerol, 0.01% bromo phenol blue, at 95°C for 5 min, the protein samples were used in SDS-PAGE. Complete process cycle was performed at 4°C.

Fluorescence measurements

The fura-2 fluorescence of transfected HEK293T cells or isolated mouse CPECs was measured in a standard bath solution. Fura-2 loaded in the cells was excited with 340 and 380 nm wavelengths and emission monitored at 510 nm with a CCD camera (CoolSnap ES; Roper Scientific/Photometrics). Data were acquired and analyzed by IPlab software (Scanalytics). Ionomycin (5 μ M) was applied to confirm cell viability.

Fluid flow velocity measurements

These anesthetized mice were perfused with 10 mL ice-cold aCSF from left chamber of the heart. The brains were sectioned at 500 μ m thickness using vibrating blade microtome (Leica), and the sections were incubated at room temperature in standard bath solution with oxygen bubbling for at least 1 hr. In experiment, the sections were allowed to put on glass bottom culture dishes (MatTek corporation) with standard bath solution bubbled with oxygen for 1 hr. Movies were acquired at 20 frames/s (50 ms/frame) for 9.1 sec (total 182 frames) using a digital high-speed CCD camera, HAS-220 (Ditect Co.). Each frame was digitized into 640 \times 480 pixels with an 8 bit gray scale. Data were analyzed by imageJ.

4. Results

Expression pattern of *Trpv4*

The expression pattern of *Trpv4* was investigated using *in situ* hybridization. *Trpv4* mRNA was detected in the choroid plexus of mouse brain (Fig. 1a). The signal for *Trpv4* in the choroid plexus was the strongest among the positive regions. TRPV4 protein expression in the choroid plexus was observed by immunohistochemistry in wild-type (WT), but not in TRPV4-deficient (TRPV4KO) mice (Fig. 1b). The signal was the highest in the choroid plexus. These results suggested that TRPV4 expression in the choroid plexus was the highest in the mouse brain. To confirm this expression pattern, transgenic mice carrying a bacterial artificial chromosome which expressed the enhanced green fluorescent protein (EGFP) in TRPV4-positive cells were generated (Fig. 1c). In theory, EGFP was continuously expressed after a single transcription, because the tetracycline response element (TRE) and mammalianized tetracycline transactivator (mtTA) are connected with the 2A peptide. The 2A peptide is formed by 21 amino acid residues, and peptide binding is separated in translation³⁴. Therefore, efficient EGFP expression should not depend on endogenous transcription activity in the transgenic mice (Fig. 1d). However, this system did not work as anticipated in mice although it worked in HEK293T cells. Accordingly, EGFP expression likely depended on the endogenous transcriptional activity in the transgenic mice. As expected, EGFP expression was observed in the choroid plexus (Fig. 1e). Thus, TRPV4 expression in the choroid plexus was confirmed in three different histological analyses.

Efforts were made to determine TRPV4 localization in the choroid plexus. Several membrane proteins such as aquaporin 1 (AQP1) and anion exchanger 2 are known to be localized to restricted areas of CPECs³⁵. Similarly, TRPV4 localization in the apical membrane has been suggested in

previous report although the co-localization with an apical marker was not investigated²³. Hence, the author tried to confirm the localization of TRPV4 protein in CPECs with an apical membrane marker of CPECs, Na/K ATPase $\alpha 1$. TRPV4 signals detected with an anti-TRPV4 antibody using a confocal microscope overlapped with those observed with an anti-Na/K ATPase $\alpha 1$ antibody in CPECs (Fig. 2b). This result suggested that TRPV4 was localized in the apical membrane of CPECs.

Functional expression of TRPV4 in CPECs

Because Na/K ATPase $\alpha 1$ is observed only in epithelial cells by immunohistochemistry, Na/K ATPase $\alpha 1$ expression was used as a marker for CPECs (Fig. 3a). In choroid plexus cell suspensions, the author noted both small (4.5 to 7.0 μm) and large (8.0 to 10.5 μm) cells (Fig. 3b). Only large cells expressed Na/K ATPase $\alpha 1$, indicating that cells with a diameter over 8.0 μm could be classified as CPECs (Fig. 3c) although both large and small cells responded to a TRPV4 agonist, GSK1016790A (GSK) in a calcium-imaging experiment (Fig. S2). The results suggested that the large cells were epithelial cells and the small cells were endothelial cells. Cell capacitance proportionally corresponds to the cell size, and small cells under the microscope had capacitance of approximately 5 to 10 pF. Accordingly, large cells with a capacitance of approximately 20 to 30 pF were used for the following patch-clamp recordings.

The TRPV4-mediated responses to 0.1 μM GSK were analyzed in whole-cell patch-clamp recordings because an EC_{50} value of approximately 0.3 μM was seen in HEK293T cells expressing mouse TRPV4 (Fig. 4a). GSK-evoked currents with an outwardly rectifying current-voltage (I-V) relationship were observed in CPECs (Fig. 4b upper) whereas such currents were not observed in CPECs isolated from TRPV4KO mice even with a high concentration of GSK (1 μM) (Fig. 4b lower).

These results indicated the expression and function of TRPV4 in the plasma membrane of CPECs.

Currents of calcium-activated chloride channels in CPECs

Calcium entering the cells through TRPV4 might affect the function of calcium-dependent proteins. For instance, it was recently reported that TRPV4 interacts with the intermediate or small conductance calcium-activated potassium channels in endothelial cells³². Nonetheless, TRPV4 could also interact with calcium-activated chloride channels, the functional expression of which has not yet been documented in CPECs³⁶. Therefore, calcium-activated chloride currents were examined using NMDG chloride for both bath and pipette solutions. Outwardly rectifying chloride currents were observed with 500 nM intracellular free calcium and the currents were inhibited by a broad chloride channel blocker, 5-nitro-2-(3-phenylpropylamino) benzoic acid (NPPB) (Fig. 4c), suggesting the existence of calcium-activated chloride channels in CPECs. The existence of calcium-activated chloride channels was confirmed with a calcium ionophore, ionomycin. Ionomycin-induced chloride currents were observed after a long delay (probably due to the time required for increases in cytosolic calcium concentration). The currents were also inhibited by NPPB (Fig. 4d). These results indicated the functional expression of calcium-activated chloride channels with outward rectification in CPECs.

Expression pattern of *Ano1* in CPECs

The author next examined the expression of genes encoding anoctamins that were recently documented in calcium-activated chloride channels³⁷⁻³⁹. Among the anoctamin family of proteins, anoctamin 1 (ANO1) has the highest calcium sensitivity based on an acidic cluster (444-EEEEEE-448) and four amino acid residues (449-EAVK-452)⁴⁰ between transmembrane two and three. And the activation is

known to peak within a few seconds³⁷⁻³⁹. Because such properties are favorable for functional interaction with TRPV4, the author was prompted to first examine *Ano1* mRNA expression. A clear amplified band corresponding to *Ano1* fragment was observed in samples from both WT and TRPV4KO LVCP (Fig. 5a). Similar amplified bands were observed in the choroid plexus from the fourth (4VCP) and the third (3VCP) ventricles (Fig. 5b). ANO1 protein expression was confirmed by immunohistochemistry in WT LVCP (Fig. 5c). The expression of other anoctamin subtypes was tested in 4VCP, 3VCP and LVCP. mRNAs for *Ano4*, *Ano6* and *Ano10* were detected in 4VCP, 3VCP and LVCP, whereas mRNA expression of *Ano3* isoform1 and *Ano8* was observed in only some of the choroid plexuses (Fig. 5d and Table 2). Thus, ANO1, ANO6 and ANO10 are candidate calcium-activated chloride channels that could be activated by calcium entering the cells through TRPV4. On the other hand, calcium-insensitive ANO4 is not a likely candidate for calcium-activated chloride channels although *Ano4* mRNA is well expressed in choroid plexus.

Current properties of ANO1-mediated currents

In order to characterize the calcium-activated chloride currents in HEK293T cells expressing ANO1, step-pulses from -100 mV to +100 mV with 20 mV increments were applied for 500 ms from the holding potential of 0 mV in whole-cell patch-clamped cells (Fig. 6). No currents were observed with the intracellular free calcium concentration. The outward currents became larger with slow activating kinetics at very positive potentials and inward currents became smaller with time-dependent desensitization especially at very negative potentials at 300 nM intracellular free calcium. When the intracellular free calcium concentration was raised over 500 nM, the activated currents showed a linear I-V relationship without desensitization. These properties with intracellular free calcium-dependent

changes in the I-V relationship are consistent with those reported for cloned anoctamins.

Functional linkage between TRPV4 and ANO1

ANO1 was the most likely candidate expressed in CPECs among the three anoctamins (ANO1, ANO6 and ANO10) in CPECs because ANO1 has high calcium sensitivity^{38,41}. To investigate ANO1-mediated currents with TRPV4 activity, whole-cell patch-clamp recordings were conducted on HEK293T cells expressing TRPV4 and ANO1, or TRPV4 alone. Robust ANO1-mediated currents were observed upon TRPV4 activation by 0.1 μ M GSK with 100 nM intracellular free calcium, while no GSK-induced currents were observed in HEK293T cells expressing ANO1 alone (Fig.7 a). In contrast, large GSK-induced chloride currents were not observed in cells expressing TRPV4 with either ANO4, ANO6 or ANO10 (Fig. 7b). These results suggested that TRPV4 activation was linked with ANO1, but not with ANO4, ANO6 or ANO10. The author speculated that calcium entering the cells through TRPV4 activated ANO1. If this were the case, functional linkage between TRPV4 and ANO1 should be extracellular calcium-dependent. In order to examine the possibility, GSK-induced ANO1-mediated currents both zero and 2 mM extracellular calcium conditions were compared. In this investigation, ANO1-mediated currents were observed upon TRPV4 activation by 0.1 μ M GSK with 100 nM intracellular free calcium in the presence of extracellular calcium but not in the absence of extracellular calcium (Fig. 7c), supporting the author's idea. Moreover, it is well known that TRPV4 can bind to some proteins, including AQP4, AQP5 and β -catenin^{15,42-44}. Therefore, the possibility of physical interaction between TRPV4 and ANO1 in HEK293T cells was pursued with immunoprecipitation. However, clear evidence of physical interaction between them could not be obtained (Fig. 7d). Those results suggested that the functional linkage depend on an indirect pathway

through TRPV4-mediated calcium influx. Next, the author investigated whether similar GSK-induced chloride currents could be observed in the presence of 2 mM extracellular calcium in native CPECs. GSK-induced chloride currents were observed in CPECs in the absence of T16inh-A01 (A01), an inhibitor of ANO1 and ANO2⁴⁵, but not in the presence of A01 (Fig. 8). Because *Ano2* mRNA was not observed in choroid plexus, a functional linkage between TRPV4 and ANO1 in CPECs was indicated.

Heat-evoked chloride currents in CPECs

ANO1 was recently shown to be activated by noxious heat in primary sensory neurons⁴⁶. The presence of heat-evoked ANO1-mediated currents with outward rectification in HEK293T cells was confirmed (Fig. 9a and b). The heat-evoked chloride currents continuously increased with the rise in temperature up to 42°C (Fig. 9b). Hence, the author investigated heat-evoked chloride currents in isolated CPECs of WT and TRPV4KO mice. Similar heat-evoked chloride currents were seen in both in WT and TRPV4KO CPECs. Interestingly, the heat-evoked chloride currents were markedly increased after GSK application even in the presence of a TRPV4-specific inhibitor, HC067047 (HC06) in WT CPECs. However, the GSK-induced enhancement of the heat-evoked chloride currents was not observed in TRPV4KO CPECs (Fig. 9c). GSK significantly enhanced heat-evoked chloride currents in WT CPECs at a +90 mV membrane potential (Fig. 9d). These results indicated the possibility that heat-sensitivity of ANO1 was enhanced by TRPV4 activation in CPECs. However, the enhanced currents were not completely blocked by A01. Thus, the possibility of another heat-activated chloride channels also was suggested in CPECs.

5. Discussion

Production, transport and reabsorption of CSF are very important for the maintenance of the brain environment because those are the basic mechanisms for controlling the ionic balance of CSF and washing out metabolites from neurons and glial cells. The main role of CPECs is CSF production. Although the osmolalities of CSF and blood are almost the same (305 and 300 mOsm for CSF and blood, respectively)²¹, most CSF supplied from the blood is released through CPECs. The average rate of CSF production is 0.37 $\mu\text{L}/\text{mg}$ tissue min in the rabbit⁴⁷, and the total amount of CSF produced in 24 h is approximately 600 mL in humans⁴⁸. Furthermore, CSF turns over about four times per day because the total volume of the ventricle, spinal canal and subarachnoid spaces is approximately 140 mL in humans⁴⁸. Thus, CPECs should have a very effective water efflux system in order to support such rapid CSF production.

Water movement is accompanied by transcellular ion transports with various ion transporting proteins expressed in both basolateral and apical membranes of CPECs. For instance, there are Na/K/Cl co-transporters, K/Cl co-transporters and Na/K ATPase in the apical membranes, and Cl/HCO₃ exchangers, Na/H exchangers and Na/HCO₃ co-transporters on the basolateral side. In terms of Cl/HCO₃ exchangers, sodium-dependent or -independent ones have been found, and anion exchanger 2, one of the sodium-independent Cl/HCO₃ exchangers, is expressed in CPECs. The lack of the osmotic pressure difference between CSF and blood plasma suggests dynamic volume changes in the process of CSF production. Such volume changes could induce arachidonic acid production through phospholipase A₂ activation upon membrane extension⁴⁹⁻⁵¹. EET produced in a P450 monooxygenase pathway from arachidonic acid is an endogenous TRPV4 agonist⁵². Because CPECs are non-neuronal cells, calcium influx, especially increases in local calcium concentrations could have

important roles of TRPV4 activation in CPECs. As expected, calcium entering the cells through TRPV4 activated calcium-activated chloride channels. It also showed that ANO1 constituted a functional linkage between TRPV4 and calcium-activated chloride channels in CPECs. These data constitute the first description of a functional linkage between TRPV4 and calcium-activated chloride channels, and the linkage appears to be critically important for CSF production because the equilibrium potential for chloride in CPECs is approximately $-20 \text{ mV}^{19,33}$, leading to chloride efflux upon chloride channel activation, and the chloride efflux enhances water transport in CPECs. Ion transports via membrane proteins described above induces water flux through water channels, aquaporins (AQPs). Among thirteen subtypes of AQPs, AQP0, AQP1, AQP2, AQP4, AQP5, AQP8 and AQP10 are channels for water alone whereas AQP3, AQP6, AQP7 and AQP9 are channels for water plus small molecules. AQP3, AQP7 and AQP9 are permeable to glycerol and urea and AQP6 has permeability for nitrate⁵³. AQP1 and AQP4 are expressed in CPECs and AQP1 is localized on the apical side³⁵. Water flux through AQP1 depends on the osmolality gap or gravitational pressure because AQP1 are constitutively active. On the other hand, TRPV4 interacts with AQP4 that is involved in cell volume changes against hypo-osmolality⁴². Thus, activation of TRPV4 could facilitate water efflux in the apical membrane of CPECs through ANO1 activation together with AQP4 activation although AQP4 expresses in both apical and basolateral membrane. Thus, CSF production might be modulated by these mechanisms. In a model presented in Fig. 10, the apical membrane of CPEC could be extended by water influx with ion transports from the basolateral side (Phase 1). Next, TRPV4 could be activated by EET produced by PLA₂ activity at body temperature. Then, ANO1 could be activated by calcium influx through TRPV4 at body temperature (Phase 2). Finally, water efflux from CPECs could be enhanced by chloride efflux through ANO1 and cation efflux by unknown mechanisms,

possibly through cation channels (Phase 3). Thus, functional linkage between TRPV4 and ANO1 could enhance water transport from CPECs to the ventricles. This model constitutes a novel hypothesis for CSF production involving both TRPV4 and ANO1.

In addition to the transcellular water flux described above, there is a small amount of paracellular water movement through tight junctions. In the previous report, calcium influx through TRPV4 downregulated expression of claudin 1, claudin 3, claudin 4, claudin 5, claudin 7 and claudin 8 proteins in the mouse mammary cell line, HC11, but not ZO proteins⁵⁴. It suggested that TRPV4 activation enhanced transport via a paracellular pathway because claudin is critical for the maintenance of tight junctions. On the other hand, TRPV4 activation contributes to skin barrier function through cell-cell interactions, an opposing phenomenon¹⁵. Thus, TRPV4 activation could affect paracellular transport in a different manner depending on the cell types expressing TRPV4. In the case of CPECs, TRPV4 might affect ion or water transport through transcellular pathways because CPECs have very tight cell-cell junctions.

CSF-dependent maintenance of the brain environment is achieved not only by CSF production but also by other CSF-related events. Recently, some genes involved in ciliary motility in ependymal cells, including *Hydin* 3⁵⁵, *Mdnah* 5⁵⁶, *Ift 88*⁵⁷, *Celsr 2* and *Celsr 3*²⁹, have been found and it was suggested that the cilia have a critical role in hydrocephalus. Severe hydrocephalus was observed in mice lacking these genes. These observations suggest that the impairment of flow of continuously produced CSF regardless of changes in brain pressure could cause serious brain damage. Therefore, research clarifying the mechanisms of CSF production could be very important to reduce life-threatening diseases such as hydrocephalus.

Expression of *Ano4*, *Ano6*, and *Ano10* mRNAs in the choroid plexus was shown here. ANO4 is

a calcium-insensitive anoctamin, whereas ANO6 and ANO10 are calcium-activated chloride channels, as is ANO1. ANO4-mediated chloride currents were not observed in HEK293T cells expressing TRPV4 and ANO4, consistent with ANO4's lack of calcium sensitivity. On the other hand, ANO6 and ANO10 are very slowly activated over a time range of 10 min³⁸, and ANO6-mediated currents show strong outward rectification even at high activation, unlike ANO1. The findings that GSK-induced chloride currents exhibited a linear I-V relationship in CPECs and that HEK293T cells expressing TRPV4 and ANO6 or ANO10 did not provide significant chloride currents upon GSK application argue against the involvement of ANO6 or ANO10. However, the slow activation of ANO6 or ANO10 suggests that ANO6 or ANO10 might be activated over a longer time downstream of TRPV4 activation. Linkage between TRPV4 and ANO6 or ANO10 could operate in pathological conditions with high intracellular calcium concentrations upon TRPV4 over-activation. Such conditions might lead to CPEC death and immune cell reactions in the case of ANO6. ANO6 is a type of scramblase, a membrane protein translocating phosphatidylserine (an "eat-me" signal) from the inside to the outside of the plasma membrane^{58,59}, and there are many macrophage-like cells called Kolmer cells or epiplexus cells on the apical side of CPECs⁶⁰ which could eat CPECs.

ANO1 could be activated without TRPV4 activation if other cascades increased intracellular calcium concentrations. Expression of Gq protein coupled receptors (GPCRs) has been suggested in the choroid plexus, including serotonin, bradykinin and ATP receptors⁶¹⁻⁶³. Moreover, outwardly rectifying chloride currents induced by ATP application were observed in CPECs⁶⁴. In deed, the author observed that ATP increased intracellular calcium concentrations and induced outwardly rectifying chloride currents in CPECs whereas no cytosolic calcium increases were observed in response to serotonin, norepinephrine or bradykinin (Fig. S3). Thus, ANO1 could be activated

downstream of GPCRs activation. On the other hand, calcium entering the cells through TRPV4 could act on other calcium-activated channels, including bestrophin2 (*Best2*), which has calcium sensitivity, and calcium-activated potassium channels. *Best2* codes for a bicarbonate channel that was discovered as a gene responsible for vitelliform macular dystrophy^{65,66}. TRPV4, ANO1 and Best2 have been reported to be expressed in the submandibular salivary gland of mice. However, TRPV4 is expressed on the apical side of acinar cells and ANO1 is expressed on the basolateral side of acinar cells, while Best2 is expressed in granular duct cells in submandibular salivary gland^{37,67,68}. Thus, functional linkage of TRPV4 with other channels should be examined in the future in order to better understand the calcium-mediated connection between calcium-permeable channels and calcium-sensitive membrane proteins.

Basic research could lead to treatments of some brain diseases, as choroid plexus cyst and choroid plexus papilloma. Choroid plexus cysts are mainly observed in the fetus. In most cases, the cysts disappear spontaneously, however residual cysts cause severe hydrocephalus. Choroid plexus papilloma accelerates excessive production of CSF, leading to hydrocephalus. There are only palliative therapies, including external ventricular drainage or a surgical shunt to help CSF movement. Control of CSF production through regulation of TRPV4 activity could lead to safer ways to treat those diseases.

6. Acknowledgements

The author thanks Professor Makoto Tominaga who is a doctoral adviser, Professor Akihiro Yamanaka in Nagoya University and Associate Professor Koji Shibasaki in Gunma University for their advices in supports of these investigations. And the author thanks Professor Uhtaek Oh in Seoul National University for providing with anoctamin plasmid DNAs and an anti-ANO1 antibody. The author also thanks Associate Professor Hiroyuki Watanabe in Akita University, Professor Junichi Nabekura and Professor Yoshihiro Kubo at the National Institute for Physiological Sciences (NIPS). Additionally, the author thanks Professor Yasunobu Okada at the NIPS, Professor Toshihiko Fujimori at the National Institute for Basic Biology, Associate Professor Kenji F. Takana in Keio University, Assistant Professor Akihiro Imura at the Institute of Biomedical Research and Innovation Laboratory, Assistant Professor Yoshiro Suzuki and Doctor Kaori Sato-Numata at the NIPS for technical advices and the generous gifts of materials. Finally, the author thanks every member of Professor Tominaga's laboratory for their supports.

7. References

1. Caterina, M.J., *et al.* The capsaicin receptor: a heat-activated ion channel in the pain pathway. *Nature* **389**, 816-824 (1997).
2. Caterina, M.J., Rosen, T.A., Tominaga, M., Brake, A.J. & Julius, D. A capsaicin-receptor homologue with a high threshold for noxious heat. *Nature* **398**, 436-441 (1999).
3. Peier, A.M., *et al.* A heat-sensitive TRP channel expressed in keratinocytes. *Science* **296**, 2046-2049 (2002).
4. Guler, A.D., *et al.* Heat-evoked activation of the ion channel, TRPV4. *J Neurosci* **22**, 6408-6414 (2002).
5. Watanabe, H., *et al.* Heat-evoked activation of TRPV4 channels in a HEK293 cell expression system and in native mouse aorta endothelial cells. *J Biol Chem* **277**, 47044-47051 (2002).
6. Togashi, K., *et al.* TRPM2 activation by cyclic ADP-ribose at body temperature is involved in insulin secretion. *EMBO J* **25**, 1804-1815 (2006).
7. Talavera, K., *et al.* Heat activation of TRPM5 underlies thermal sensitivity of sweet taste. *Nature* **438**, 1022-1025 (2005).
8. McKemy, D.D., Neuhauser, W.M. & Julius, D. Identification of a cold receptor reveals a general role for TRP channels in thermosensation. *Nature* **416**, 52-58 (2002).
9. Story, G.M., *et al.* ANKTM1, a TRP-like channel expressed in nociceptive neurons, is activated by cold temperatures. *Cell* **112**, 819-829 (2003).
10. Liedtke, W., *et al.* Vanilloid receptor-related osmotically activated channel (VR-OAC), a candidate vertebrate osmoreceptor. *Cell* **103**, 525-535 (2000).
11. Strotmann, R., Harteneck, C., Nunnenmacher, K., Schultz, G. & Plant, T.D. OTRPC4, a nonselective cation channel that confers sensitivity to extracellular osmolarity. *Nat Cell Biol* **2**, 695-702 (2000).
12. Watanabe, H., *et al.* Activation of TRPV4 channels (hVRL-2/mTRP12) by phorbol derivatives. *J Biol Chem* **277**, 13569-13577 (2002).

13. Willette, R.N., *et al.* Systemic activation of the transient receptor potential vanilloid subtype 4 channel causes endothelial failure and circulatory collapse: Part 2. *J Pharmacol Exp Ther* **326**, 443-452 (2008).
14. Watanabe, H., *et al.* Anandamide and arachidonic acid use epoxyeicosatrienoic acids to activate TRPV4 channels. *Nature* **424**, 434-438 (2003).
15. Sokabe, T., Fukumi-Tominaga, T., Yonemura, S., Mizuno, A. & Tominaga, M. The TRPV4 channel contributes to intercellular junction formation in keratinocytes. *J Biol Chem* **285**, 18749-18758 (2010).
16. Mochizuki, T., *et al.* The TRPV4 cation channel mediates stretch-evoked Ca²⁺ influx and ATP release in primary urothelial cell cultures. *J Biol Chem* **284**, 21257-21264 (2009).
17. Mihara, H., Boudaka, A., Sugiyama, T., Moriyama, Y. & Tominaga, M. Transient receptor potential vanilloid 4 (TRPV4)-dependent calcium influx and ATP release in mouse oesophageal keratinocytes. *J Physiol* **589**, 3471-3482 (2011).
18. Shibasaki, K., Suzuki, M., Mizuno, A. & Tominaga, M. Effects of body temperature on neural activity in the hippocampus: regulation of resting membrane potentials by transient receptor potential vanilloid 4. *J Neurosci* **27**, 1566-1575 (2007).
19. Praetorius, J. Water and solute secretion by the choroid plexus. *Pflugers Arch* **454**, 1-18 (2007).
20. Cserr, H.F. & VanDyke, D.H. 5-hydroxyindoleacetic acid accumulation by isolated choroid plexus. *Am J Physiol* **220**, 718-723 (1971).
21. Damkier, H.H., Brown, P.D. & Praetorius, J. Epithelial pathways in choroid plexus electrolyte transport. *Physiology (Bethesda)* **25**, 239-249 (2010).
22. Jacobs, S., *et al.* Mice with targeted Slc4a10 gene disruption have small brain ventricles and show reduced neuronal excitability. *Proc Natl Acad Sci U S A* **105**, 311-316 (2008).
23. Masuzawa, T., Ohta, T., Kawakami, K. & Sato, F. Immunocytochemical localization of Na⁺, K⁺-ATPase in the canine choroid plexus. *Brain* **108 (Pt 3)**, 625-646 (1985).
24. Plotkin, M.D., *et al.* Expression of the Na⁽⁺⁾-K⁽⁺⁾-2Cl⁻ cotransporter BSC2 in the nervous system. *Am J Physiol* **272**, C173-183 (1997).

25. Karadsheh, M.F., Byun, N., Mount, D.B. & Delpire, E. Localization of the KCC4 potassium-chloride cotransporter in the nervous system. *Neuroscience* **123**, 381-391 (2004).
26. Lindsey, A.E., *et al.* Functional expression and subcellular localization of an anion exchanger cloned from choroid plexus. *Proc Natl Acad Sci U S A* **87**, 5278-5282 (1990).
27. Speake, T., Freeman, L.J. & Brown, P.D. Expression of aquaporin 1 and aquaporin 4 water channels in rat choroid plexus. *Biochim Biophys Acta* **1609**, 80-86 (2003).
28. Maekawa, F., *et al.* Localization of glucokinase-like immunoreactivity in the rat lower brain stem: for possible location of brain glucose-sensing mechanisms. *Endocrinology* **141**, 375-384 (2000).
29. Tissir, F., *et al.* Lack of cadherins Celsr2 and Celsr3 impairs ependymal ciliogenesis, leading to fatal hydrocephalus. *Nat Neurosci* **13**, 700-707 (2010).
30. Guirao, B., *et al.* Coupling between hydrodynamic forces and planar cell polarity orients mammalian motile cilia. *Nat Cell Biol* **12**, 341-350 (2010).
31. Silver, I., Li, B., Szalai, J. & Johnston, M. Relationship between intracranial pressure and cervical lymphatic pressure and flow rates in sheep. *Am J Physiol* **277**, R1712-1717 (1999).
32. Sonkusare, S.K., *et al.* Elementary Ca²⁺ signals through endothelial TRPV4 channels regulate vascular function. *Science* **336**, 597-601 (2012).
33. Johanson, C.E. & Murphy, V.A. Acetazolamide and insulin alter choroid plexus epithelial cell [Na⁺], pH, and volume. *Am J Physiol* **258**, F1538-1546 (1990).
34. Trichas, G., Begbie, J. & Srinivas, S. Use of the viral 2A peptide for bicistronic expression in transgenic mice. *BMC Biol* **6**, 40 (2008).
35. Speake, T., Kibble, J.D. & Brown, P.D. Kv1.1 and Kv1.3 channels contribute to the delayed-rectifying K⁺ conductance in rat choroid plexus epithelial cells. *Am J Physiol Cell Physiol* **286**, C611-620 (2004).
36. Millar, I.D., Bruce, J. & Brown, P.D. Ion channel diversity, channel expression and function in the choroid plexuses. *Cerebrospinal Fluid Res* **4**, 8 (2007).

37. Yang, Y.D., *et al.* TMEM16A confers receptor-activated calcium-dependent chloride conductance. *Nature* **455**, 1210-1215 (2008).
38. Schreiber, R., *et al.* Expression and function of epithelial anoctamins. *J Biol Chem* **285**, 7838-7845 (2010).
39. Tian, Y., *et al.* Calmodulin-dependent activation of the epithelial calcium-dependent chloride channel TMEM16A. *FASEB J* **25**, 1058-1068 (2011).
40. Xiao, Q., *et al.* Voltage- and calcium-dependent gating of TMEM16A/Ano1 chloride channels are physically coupled by the first intracellular loop. *Proc Natl Acad Sci U S A* **108**, 8891-8896 (2011).
41. Duran, C., Qu, Z., Osunkoya, A.O., Cui, Y. & Hartzell, H.C. ANOs 3-7 in the anoctamin/Tmem16 Cl-channel family are intracellular proteins. *Am J Physiol Cell Physiol* **302**, C482-493 (2012).
42. Benfenati, V., *et al.* An aquaporin-4/transient receptor potential vanilloid 4 (AQP4/TRPV4) complex is essential for cell-volume control in astrocytes. *Proc Natl Acad Sci U S A* **108**, 2563-2568 (2011).
43. Sidhaye, V.K., *et al.* Transient receptor potential vanilloid 4 regulates aquaporin-5 abundance under hypotonic conditions. *Proc Natl Acad Sci U S A* **103**, 4747-4752 (2006).
44. Liu, X., *et al.* A role for AQP5 in activation of TRPV4 by hypotonicity: concerted involvement of AQP5 and TRPV4 in regulation of cell volume recovery. *J Biol Chem* **281**, 15485-15495 (2006).
45. Namkung, W., Phuan, P.W. & Verkman, A.S. TMEM16A inhibitors reveal TMEM16A as a minor component of calcium-activated chloride channel conductance in airway and intestinal epithelial cells. *J Biol Chem* **286**, 2365-2374 (2011).
46. Cho, H., *et al.* The calcium-activated chloride channel anoctamin 1 acts as a heat sensor in nociceptive neurons. *Nat Neurosci* **15**, 1015-1021 (2012).
47. Welch, K. Secretion of Cerebrospinal Fluid by Choroid Plexus of the Rabbit. *Am J Physiol* **205**, 617-624 (1963).
48. Brown, P.D., Davies, S.L., Speake, T. & Millar, I.D. Molecular mechanisms of cerebrospinal fluid production. *Neuroscience* **129**, 957-970 (2004).

49. Thoroed, S.M., Lauritzen, L., Lambert, I.H., Hansen, H.S. & Hoffmann, E.K. Cell swelling activates phospholipase A2 in Ehrlich ascites tumor cells. *J Membr Biol* **160**, 47-58 (1997).
50. Basavappa, S., Pedersen, S.F., Jorgensen, N.K., Ellory, J.C. & Hoffmann, E.K. Swelling-induced arachidonic acid release via the 85-kDa cPLA2 in human neuroblastoma cells. *J Neurophysiol* **79**, 1441-1449 (1998).
51. Pedersen, S., Lambert, I.H., Thoroed, S.M. & Hoffmann, E.K. Hypotonic cell swelling induces translocation of the alpha isoform of cytosolic phospholipase A2 but not the gamma isoform in Ehrlich ascites tumor cells. *Eur J Biochem* **267**, 5531-5539 (2000).
52. Fleming, I. Cytochrome p450 and vascular homeostasis. *Circ Res* **89**, 753-762 (2001).
53. Liu, H. & Wintour, E.M. Aquaporins in development -- a review. *Reprod Biol Endocrinol* **3**, 18 (2005).
54. Reiter, B., *et al.* TRPV4-mediated regulation of epithelial permeability. *FASEB J* **20**, 1802-1812 (2006).
55. Lechtreck, K.F., Delmotte, P., Robinson, M.L., Sanderson, M.J. & Witman, G.B. Mutations in Hydin impair ciliary motility in mice. *J Cell Biol* **180**, 633-643 (2008).
56. Ibanez-Tallon, I., *et al.* Dysfunction of axonemal dynein heavy chain Mdnah5 inhibits ependymal flow and reveals a novel mechanism for hydrocephalus formation. *Hum Mol Genet* **13**, 2133-2141 (2004).
57. Banizs, B., *et al.* Dysfunctional cilia lead to altered ependyma and choroid plexus function, and result in the formation of hydrocephalus. *Development* **132**, 5329-5339 (2005).
58. Suzuki, J., Umeda, M., Sims, P.J. & Nagata, S. Calcium-dependent phospholipid scrambling by TMEM16F. *Nature* **468**, 834-838 (2010).
59. Yang, H., *et al.* TMEM16F forms a Ca²⁺-activated cation channel required for lipid scrambling in platelets during blood coagulation. *Cell* **151**, 111-122 (2012).
60. Shimada, T., Ko, K.-D. & Murakami, M. Scanning and transmission electron microscopic observations of epiplexus cells (Kolmer cells) in monkey brain. *Kurume Medical Journal* **22**, 17-22 (1975).
61. Kaufman, M.J., Hartig, P.R. & Hoffman, B.J. Serotonin 5-HT_{2C} receptor stimulates cyclic GMP formation in choroid plexus. *J Neurochem* **64**, 199-205 (1995).

62. Chen, E.Y., Emerich, D.F., Bartus, R.T. & Kordower, J.H. B2 bradykinin receptor immunoreactivity in rat brain. *J Comp Neurol* **427**, 1-18 (2000).
63. Johansson, P.A., *et al.* Expression and localization of P2 nucleotide receptor subtypes during development of the lateral ventricular choroid plexus of the rat. *Eur J Neurosci* **25**, 3319-3331 (2007).
64. Schwiebert, E.M., *et al.* CFTR regulates outwardly rectifying chloride channels through an autocrine mechanism involving ATP. *Cell* **81**, 1063-1073 (1995).
65. Petrukhin, K., *et al.* Identification of the gene responsible for Best macular dystrophy. *Nat Genet* **19**, 241-247 (1998).
66. Yu, K., Lujan, R., Marmorstein, A., Gabriel, S. & Hartzell, H.C. Bestrophin-2 mediates bicarbonate transport by goblet cells in mouse colon. *J Clin Invest* **120**, 1722-1735 (2010).
67. Zhang, Y., Catalan, M.A. & Melvin, J.E. TRPV4 activation in mouse submandibular gland modulates Ca²⁺ influx and salivation. *Am J Physiol Gastrointest Liver Physiol* **303**, G1365-1372 (2012).
68. Romanenko, V.G., *et al.* Tmem16A encodes the Ca²⁺-activated Cl⁻ channel in mouse submandibular salivary gland acinar cells. *J Biol Chem* **285**, 12990-13001 (2010).

8. Tables

Table 1

Primer list for reverse transcription-PCR (RT-PCR). All primers span an exon-exon junction.

Table 1

ANO	forward	reverse
1	TTCGTCAATCACACGCTCTC	CTGCTCCTCACGCATAAACA
2	GACAGAAAGCTGCTGTATCA	TTTCATATTCAGGCCGAGAG
3_1	AAAGCAGGTGTCAGATTGCG	TTTCCCAGAGCCAAGCAAAA
3_2	ACGCGACTTCTTGTGTCTGT	GGGTGGCCTACGAATCTTCC
4	CGACCCAGTTTGAAGCCAA	GGGTGGCACTCTTCTAGCCT
5	ATGGAATCCGGCAGATCGAC	ATACTGGCCATCATGGAGCG
6	CTGGGCACCCACAAGAGTAT	GATGATCCCCATGTTTTTGG
7	CAGCACCAAGAGGCATCAGA	GCTCCTGCGTTGGTATGTCT
8	AATTGAGGTTTGGCTTGGGC	GAGCAGGCTCTCGTATGTGG
9	AGGTACCGGGACTACCGAAA	TGAAGCGCATTCTATGGCGA
10	TCGATATGCTGCCGAGTTCC	AAAAGCCAACTGCCATACGC

Table 2

Summary of RT-PCR results for ANOs. *Ano1*, *Ano4*, *Ano6* and *Ano10* were detected in the fourth, the third and the lateral ventricles. (+), (-) and (\pm) indicate expression, no-expression and equivocal expression, respectively.

Table 2

ANO	4th ventricle	3rd	lateral
1	+	+	+
2	-	-	-
3_1	\pm	-	+
3_2	-	-	-
4	+	+	+
5	-	-	\pm
6	+	+	+
7	-	-	-
8	+	-	+
9	-	-	-
10	+	+	+

9. Figure Legends

Figure 1

Histological analysis for *Trpv4* and generation of TRPV4/EGFP transgenic mice.

(a) Micrographs of *in situ* hybridization in the sagittal section of wild-type (WT) mouse brain. *Trpv4* mRNA with an antisense probe was detected in the choroid plexus, but not with a sense probe. Arrowheads indicate a lateral ventricle choroid plexus. (b) Fluorescence micrographs of immunohistochemistry in the coronal section of WT and TRPV4-deficient (TRPV4KO) mouse brains. A TRPV4-positive signal was detected in the choroid plexus of WT, but not in TRPV4KO mice. An arrowhead indicates a third ventricle choroid plexus. (c) Strategy for generating TRPV4/EGFP transgenic mice. A DNA allele was recombined at exon 2 of *Trpv4* in a bacterial artificial chromosome. This allele contained a tetracycline response element (TRE), EGFP, 2A sequence and mammalianized tetracycline transactivator (mtTA) labeled by c-Myc. (d) A model of EGFP enhancement. Both EGFP and mtTA were expressed by a single transcription of *Trpv4*. Then, these peptides were separated at 2A peptide in translation. The separated mtTA moved into the nucleus, and the DNA allele was transcribed again by TRE recognition of mtTA. Thus, EGFP expression continued to be induced independently of native transcriptional activity. (e) Fluorescence micrographs of immunohistochemistry for EGFP in the sagittal section of the transgenic and WT mouse brain. EGFP expression was shown with an anti-GFP antibody in the choroid plexus of transgenic mice, but not in WT mice. An arrowhead indicates a lateral ventricle choroid plexus.

Figure 2

Expression pattern of TRPV4 in choroid plexus.

(a) A schematic model of the choroid plexus structure. This tissue consists of epithelial cells, leptomeninges and fenestrated capillaries. The epithelial cells constitute a monolayer, and there are tight junctions between cells that form a blood-cerebrospinal fluid (CSF) barrier as a result of which the epithelial cell is separated into apical and basolateral sides. (b) Confocal micrographs of double staining of Na/K ATPase $\alpha 1$ and TRPV4. Na/K ATPase $\alpha 1$ is an apical marker in choroid plexus epithelial cells (CPECs). TRPV4 staining was completely merged with Na/K ATPase $\alpha 1$.

Figure 3

Classification of cells isolated from the choroid plexus of the lateral and the fourth ventricles.

An anti-Na/K ATPase $\alpha 1$ antibody was used to selectively visualize CPECs. (a) Fluorescence micrographs in the sagittal section of WT mouse brain. (b) Immunocytochemistry for Na/K ATPase $\alpha 1$ (red) and DAPI (blue) in isolated CPECs. There are two types of cells, Na/K ATPase $\alpha 1$ -positive and -negative cells. Black arrowheads indicate the positive cells, and white arrowheads indicate the negative cells. (c) Size distribution of Na/K ATPase $\alpha 1$ -positive cells. Diameters of the positive cells ranged from 8.0 to 10.5 μm , and diameters of the negative cells ranged from 4.5 to 7.0 μm (left). Data represent means \pm SEM (right, $n = 10$). Statistical significance was determined by a Student's *t*-test.

Figure 4

Whole-cell patch-clamp recordings.

(a) A dose response curve of GSK1016790A (GSK)-induced activation of mouse TRPV4 in HEK293T cells. The EC₅₀ value was approximately 0.3 μ M. Filled black symbols represent means \pm SEM, and blue symbols represent individual measured values (n = 5). The data were fitted with a Hill equation.

(b) GSK responses in CPECs of WT and TRPV4KO mice. Outwardly rectifying currents (inset) induced by 0.1 μ M GSK were observed in CPECs of WT, but not in TRPV4KO mice. Standard bath and pipette solutions were used in (a) and (b). Holding potential was -60 mV and ramp-pulse was from -100 to +100 mV for 300 ms duration.

(c) Outwardly rectifying chloride currents (inset) were observed in the presence of 500 nM intracellular free calcium. The currents were inhibited by a broad chloride channel blocker, 5-nitro-2-(3-phenylpropylamino) benzoic acid (NPPB).

(d) Outwardly rectifying chloride currents (inset) were observed upon application of 5 μ M ionomycin. The currents were inhibited by NPPB. NMDG-Cl bath and pipette solutions were used in (c) and (d). Holding potential was 0 mV in (c) and -60 mV in (d), and ramp-pulse was from -100 to +100 mV for 300 ms duration.

Figure 5

Expression pattern of anoctamin (ANO) in the choroid plexuses of WT and TRPV4KO mice.

(a, b) RT-PCR for *Ano1* in the choroid plexuses of the lateral, the fourth and the third ventricles. (+) and (-) represent the PCR products with and without reverse transcription, respectively. Expected sizes for *Ano1* and *b-actin* were 330 bp and 573 bp, respectively.

(c) Confocal micrographs of immunohistochemistry with an anti-ANO1 antibody in the sagittal section of the lateral ventricle

choroid plexus. (d) RT-PCR for the other ANOs (*Ano2* - *Ano10*). Amplified fragments of *Ano4*, *Ano6* and *Ano10* were clearly observed in the three parts of the choroid plexus. Expected sizes for *Ano2*, *Ano3* isoform1, *Ano3* isoform2, *Ano4*, *Ano5*, *Ano6*, *Ano7*, *Ano8*, *Ano9* and *Ano10* are 490, 465, 368, 512, 548, 236, 398, 544, 214 and 547 bp, respectively.

Figure 6

Electrophysiological properties of ANO1.

(a) Typical traces of ANO1-mediated currents in several concentrations (0, 300 and 1000 nM) of intracellular free calcium. Step pulses for 500 msec were applied between -100 and +100 mV with 20 mV increments from 0 mV. NMDG-Cl bath and pipette solutions were used in these recordings, and the pipette solution contained 5 mM BAPTA. (b) Current - voltage (I-V) relationships for ANO1 currents at the beginning (left) and ending (right) of the step pulses indicated by arrowheads (n = 5).

Figure 7

Whole-cell patch-clamp recordings in HEK293T cells and CPECs.

(a) ANO1-mediated currents induced by 0.1 μ M GSK in HEK293T cells expressing TRPV4 and ANO1 (violet, n = 5), cells expressing TRPV4 alone (cyan, n = 9) and cells expressing ANO1 alone (green, n = 5) at -50 or +50 mV membrane potential. Representative current traces in cells expressing TRPV4 and ANO1 (red) and cell expressing TRPV4 alone (black) are shown in the inset. (b) Comparison of the currents upon 0.1 μ M GSK treatment in cells expressing TRPV4 and ANO4 (yellow, n = 4), cells expressing TRPV4 and ANO6 (green, n = 4), cells expressing TRPV4 and ANO10 (magenta, n = 8) and cells TRPV4 alone (cyan, n = 9). (c) ANO1-mediated currents induced by 0.1

μ M GSK treatment in HEK293T cells expressing TRPV4 and ANO1 in the presence (2 mM, violet, n = 5) and absence (cyan, n = 5) of extracellular calcium. Representative current traces in presence (red) and absence (blue) are shown in the inset. Statistical significances were determined with Bonferroni correction in (a) and (b) or Student's *t*-test in (c). All data were collected using NMDG-Cl pipette solution containing 100 nM free calcium. Holding potential was -60 mV and ramp-pulse was from -100 to +100 mV for 300 ms duration. (d) Immunoprecipitation (IP) of ANO1 and Western blot (WB) for TRPV4 in cells expressing TRPV4 and ANO1 (lane 1) and cells transfected with pcDNA3.1 plasmid alone (lane 2). IP of TRPV4 and WB for TRPV4 in cells expressing TRPV4 alone (lane 3). No TRPV4 band was observed in cells expressing the two proteins.

Figure 8

(a) Whole-cell patch-clamp recordings in CPECs of WT mice. GSK-induced chloride currents were not observed in the presence of an ANO1/ANO2 blocker, T16inh-A01 (A01) (lower). (b) Data represent means \pm SEM of the absence (n = 4) and presence (n = 6) of A01. Statistical significances were determined with Student's *t*-test. All data were collected using NMDG-Cl pipette solution containing 100 nM free calcium. Holding potential was -60 mV and ramp-pulse was from -100 to +100 mV for 300 ms duration.

Figure 9

Heat-evoked chloride currents in HEK293T cells and CPECs.

(a) Representative trace of ANO1-mediated currents evoked by heating from 24 to 44°C in HEK293T cells expressing ANO1 alone. (b) The heat-evoked currents gradually increased with a rise in temperature up to 42°C. (c) A typical trace of heat-evoked chloride currents in CPECs of WT and TRPV4KO mice. Heat responses were observed in both CPECs, however the heat-evoked chloride currents increased after 0.1 μM GSK application in WT CPECs, but not in TRPV4KO CPECs. (d) Statistical analysis of the heat-evoked chloride currents. Increase in the heat-evoked chloride currents was significantly larger in WT CPECs compared with TRPV4KO CPECs. Data represent means ± SEM (n = 3). All data were collected using NMDG-Cl pipette solution containing 100 nM free calcium. Holding potential was -60 mV and ramp-pulse was from -100 to +100 mV for 300 ms duration.

Figure 10

A proposed model for CSF production in CPECs.

(Phase 1) The apical membrane of CPECs is swollen from water influx. (Phase 2) Arachidonic acid cascade is accelerated by extension of the membrane, and endogenous TRPV4 agonist, epoxyeicosatrienoic acid (EET), is produced. The EET and body temperature activate TRPV4. Then, ANO1 is activated by synergistic effects of calcium influx via TRPV4 activity and temperature. (Phase 3) Water efflux through aquaporin 1 (AQP1), which is localized in the apical membrane, is enhanced by chloride and some cations efflux that depends on the Donnan equilibrium.

Figure S1

Fluid flux velocity measurements by motile cilia in ependymal cells.

(a) Micrograph in ventricle surface. There are a lot of ependymal cells having motile cilia. (b) Representative images of fluorescence beads trajectory for 9.1 sec in the third and the lateral ventricle of sagittal sections. Left side is frontal and upper side is dorsal in these photographs. Arrows represent flow direction and blue lines represent trajectory of beads for 1 sec. (c) Mean \pm SEM of beads velocity in a third ventricle (n = 28) and a lateral ventricle (n = 17).

Figure S2

Changes in cytosolic calcium concentrations by GSK1016790A (GSK) in CPECs

Response to GSK1016790A (GSK, 300 nM) in CPECs. Data are normalized to the responses to ionomycin (5 μ M) and presented as means (n = 4 and 5 for large and small cells, respectively).

Figure S3

Changes in cytosolic calcium concentrations by several agonists for GPCRs in CPECs.

(a) Responses to serotonin (5-HT, 10 μ M), norepinephrine (NE, 10 μ M), bradykinin (BK, 10 μ M) or GSK (300 nM) in CPECs. Data are means (n = 8 (left) and n = 6 (right)). (b) 100 μ M ATP-induced increases in cytosolic calcium concentrations in CPECs. Data are means (n = 5) (c) Whole-cell chloride current in CPECs. An outwardly rectifying chloride current was induced by 100 μ M extracellular ATP. This current was collected using NMDG-Cl bath and pipette solutions. Holding potential was 0 mV and ramp-pulse was from -100 to +100 mV for 300 ms duration.

Figure 1

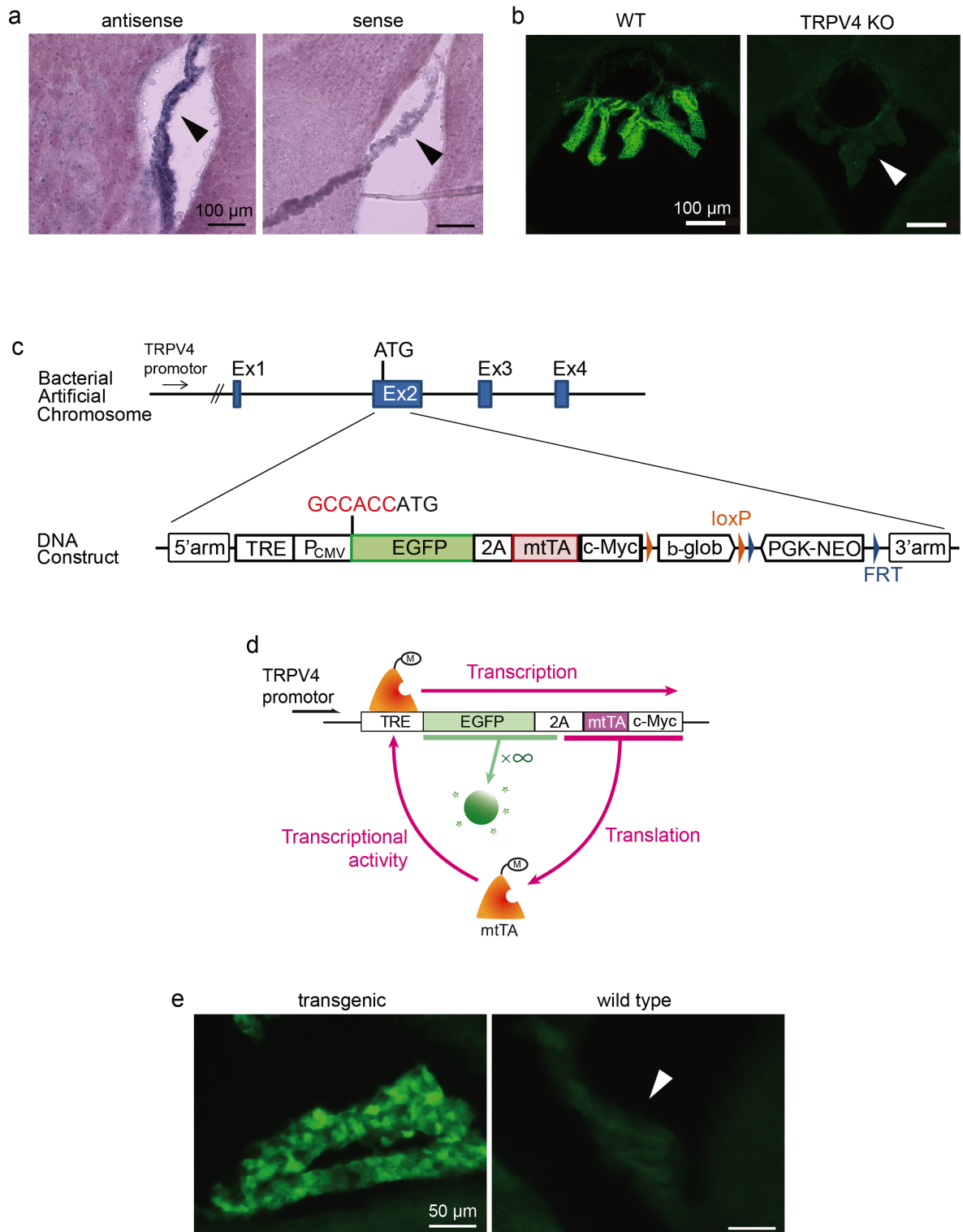


Figure 2

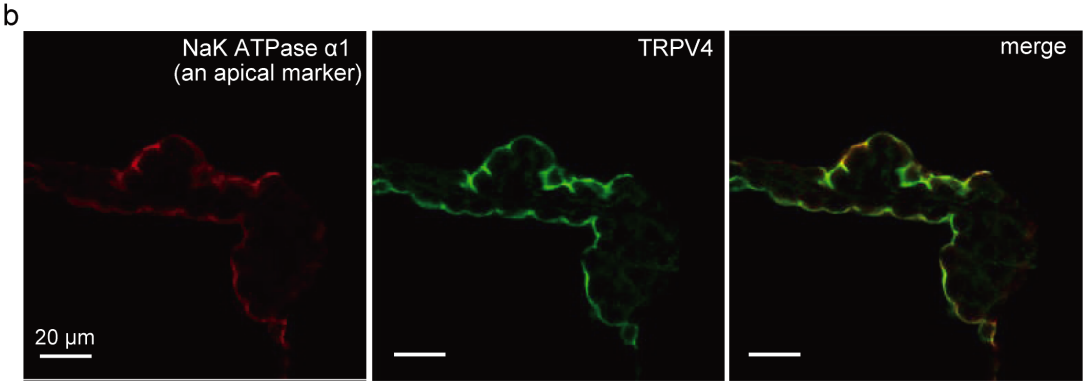
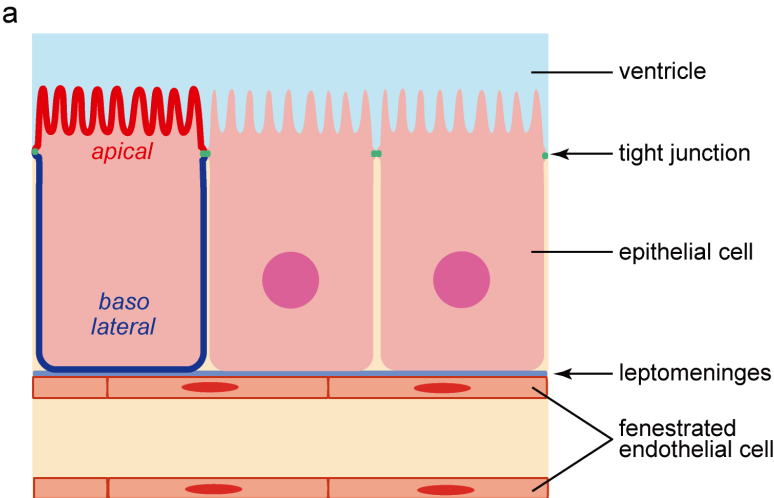


Figure 3

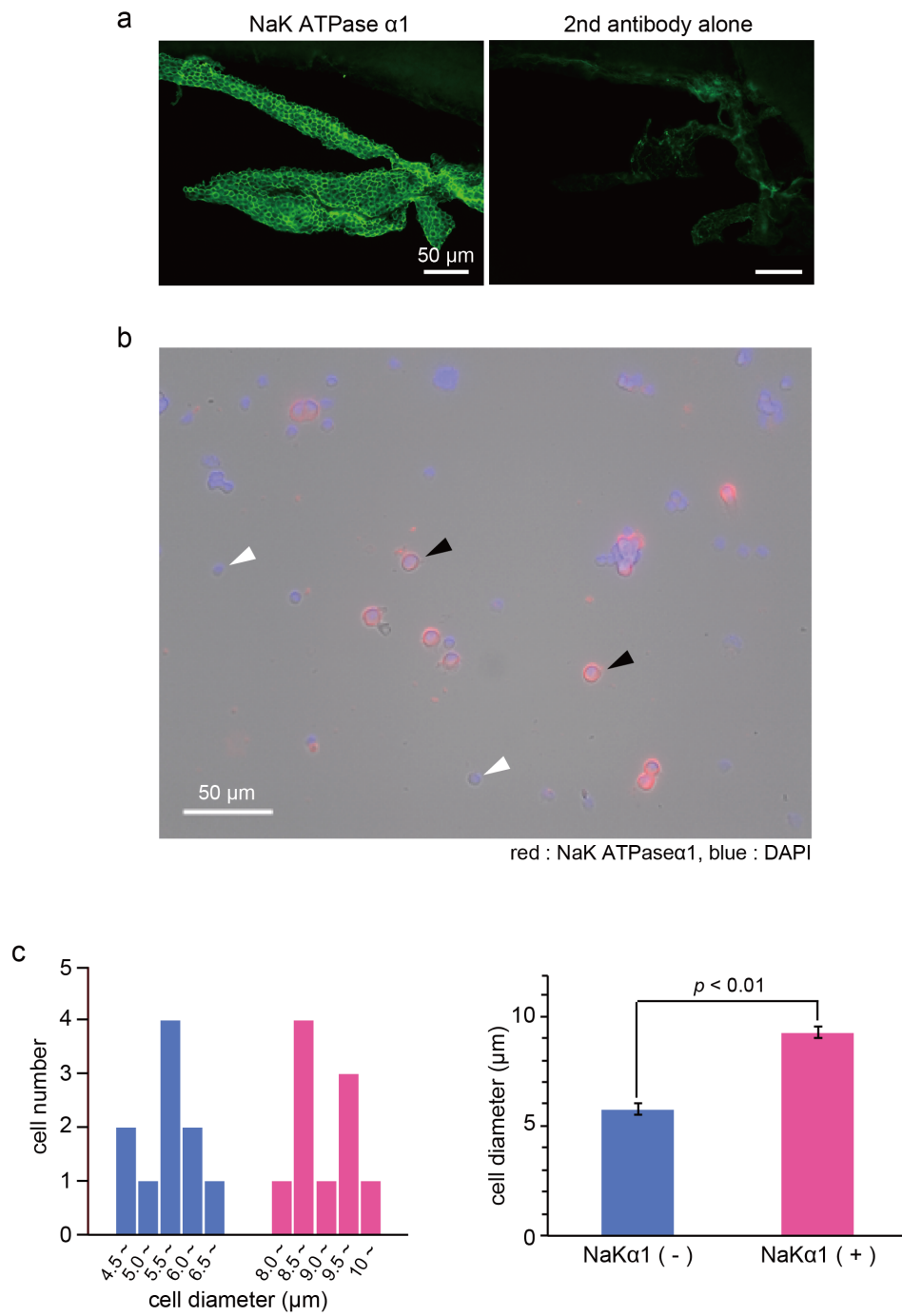


Figure 4

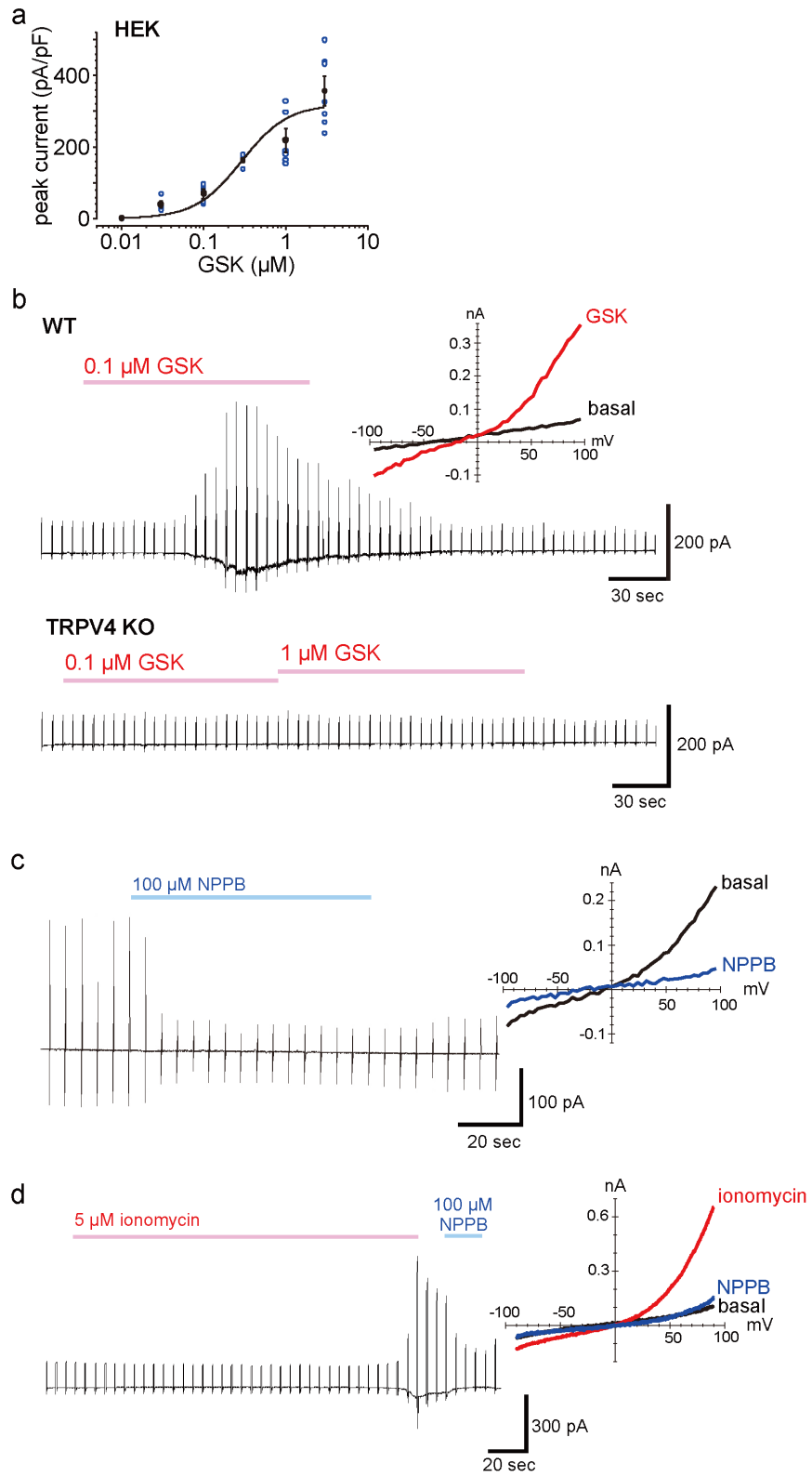


Figure 5

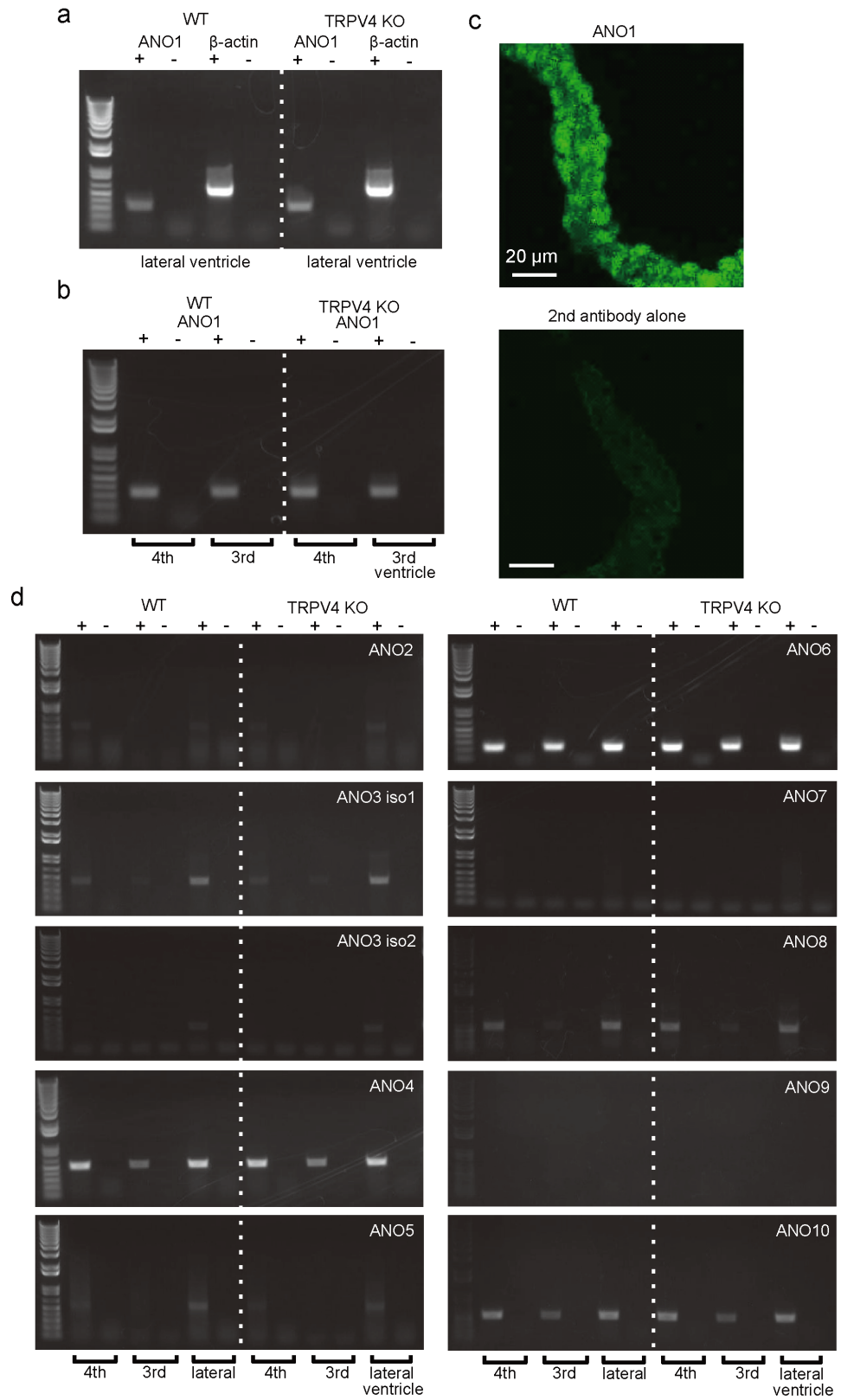


Figure 6

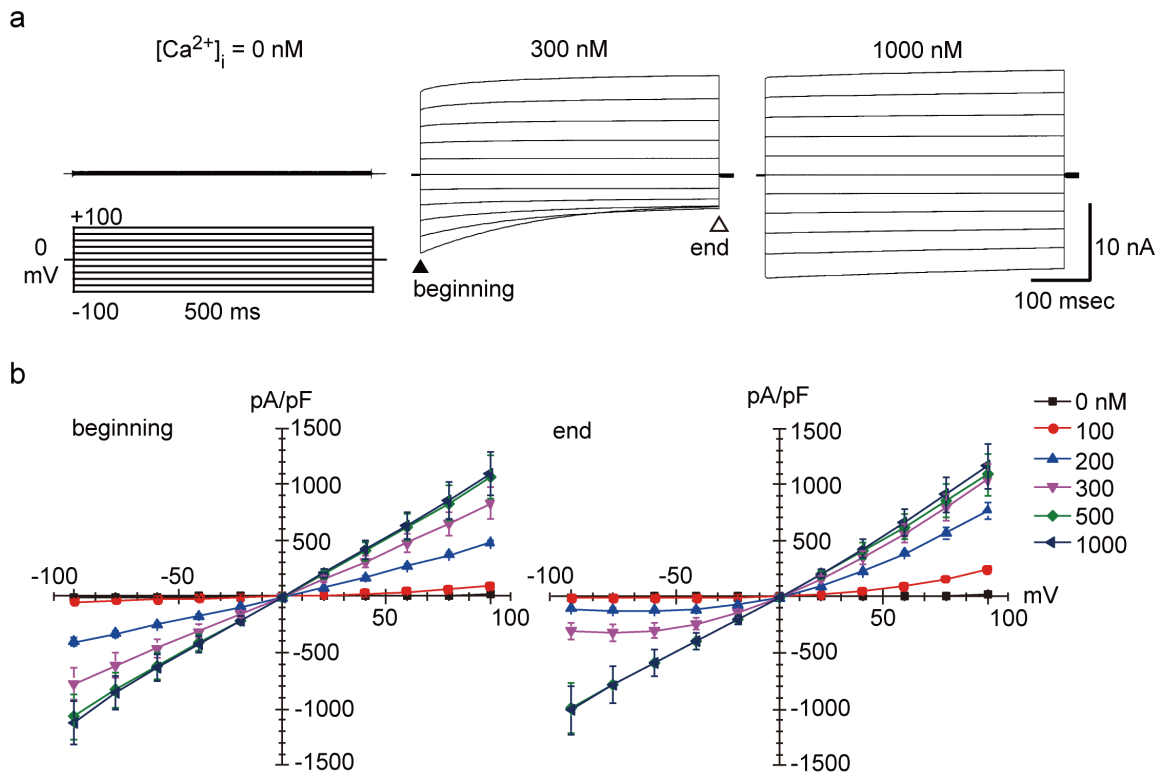


Figure 7

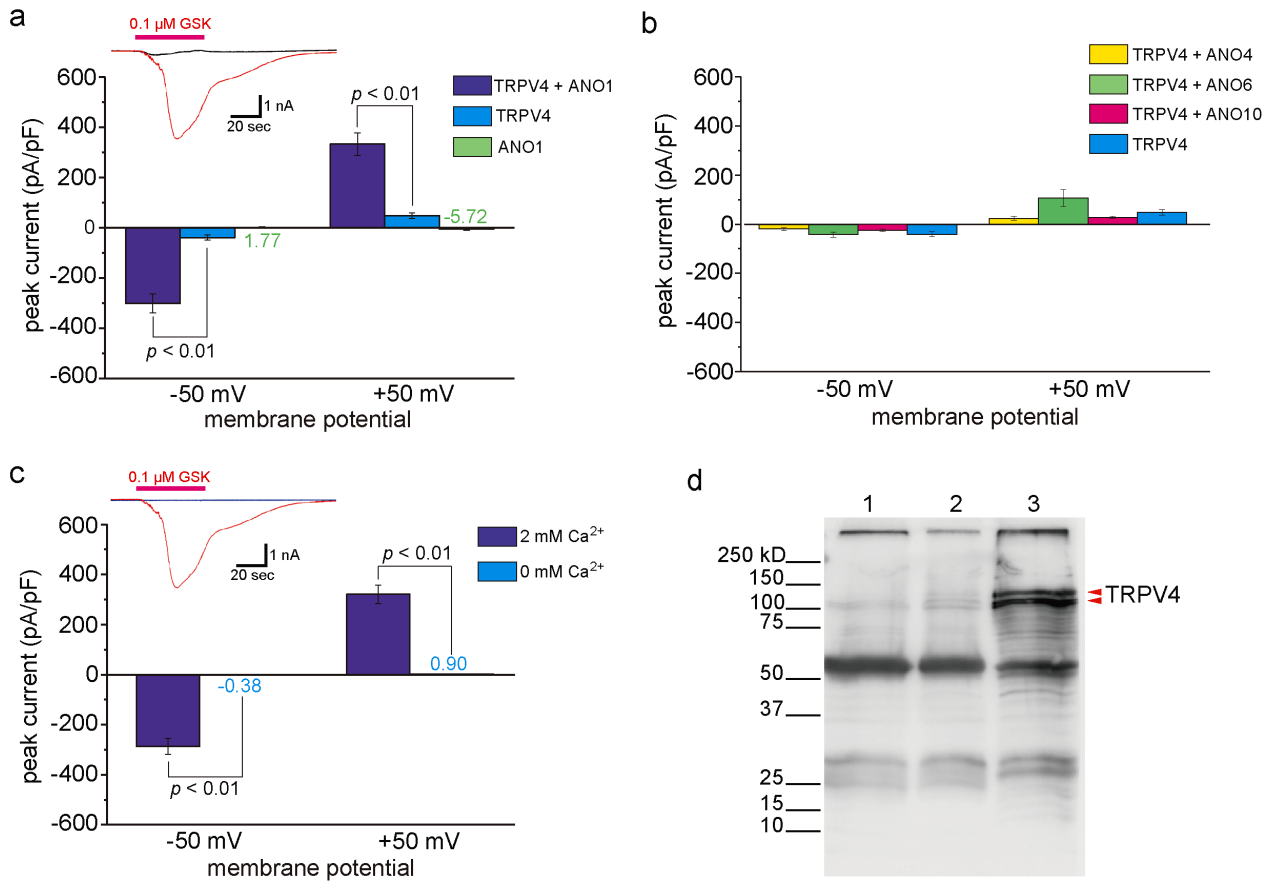
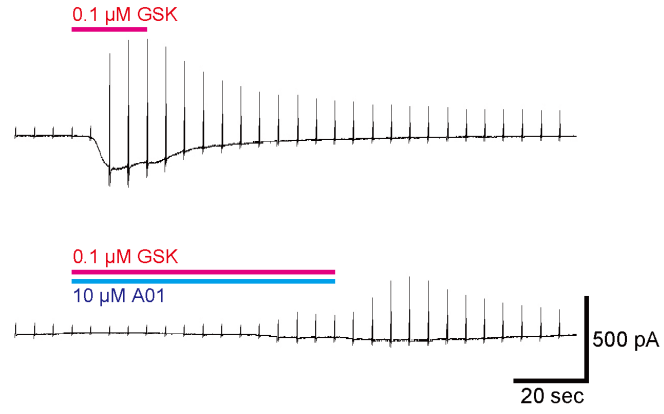


Figure 8

a



b

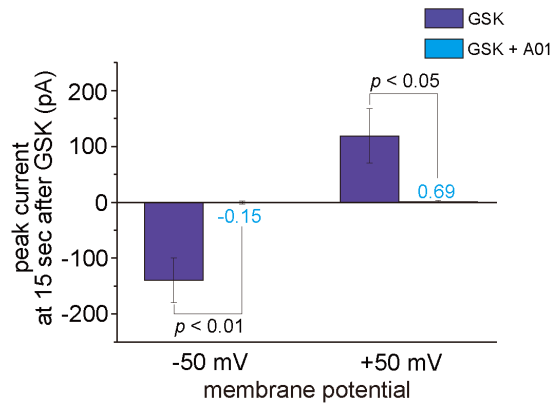


Figure 9

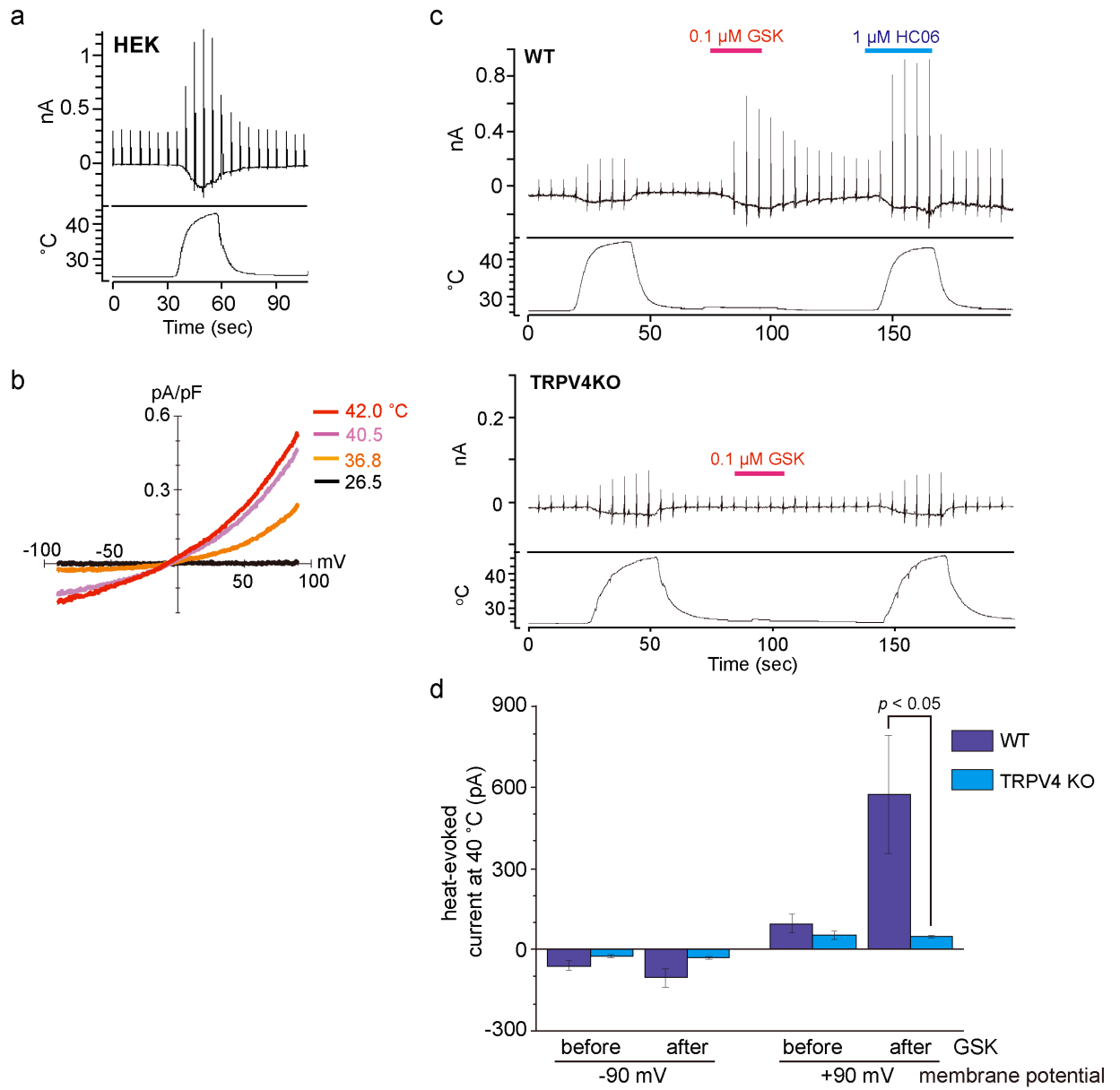


Figure 10

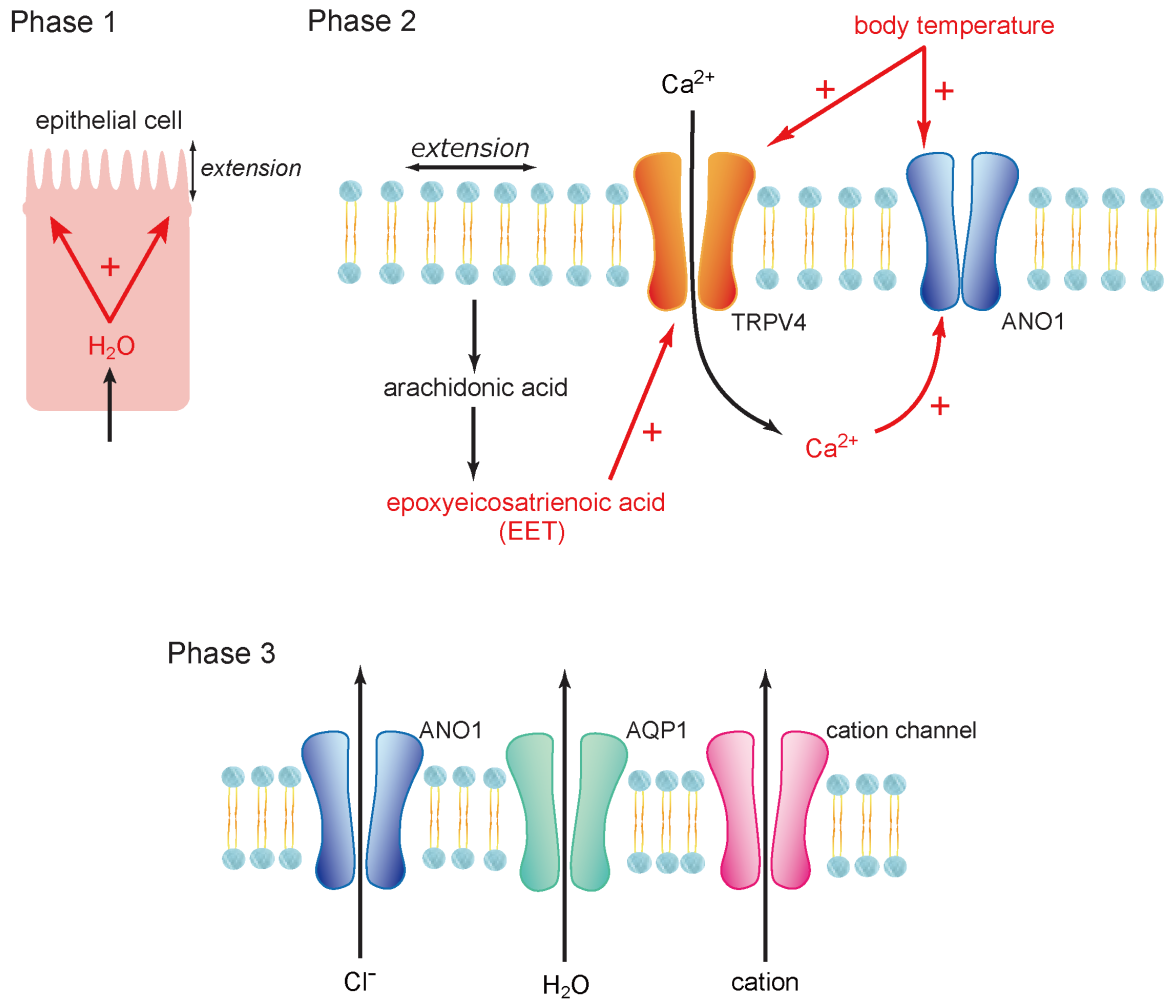


Figure S1

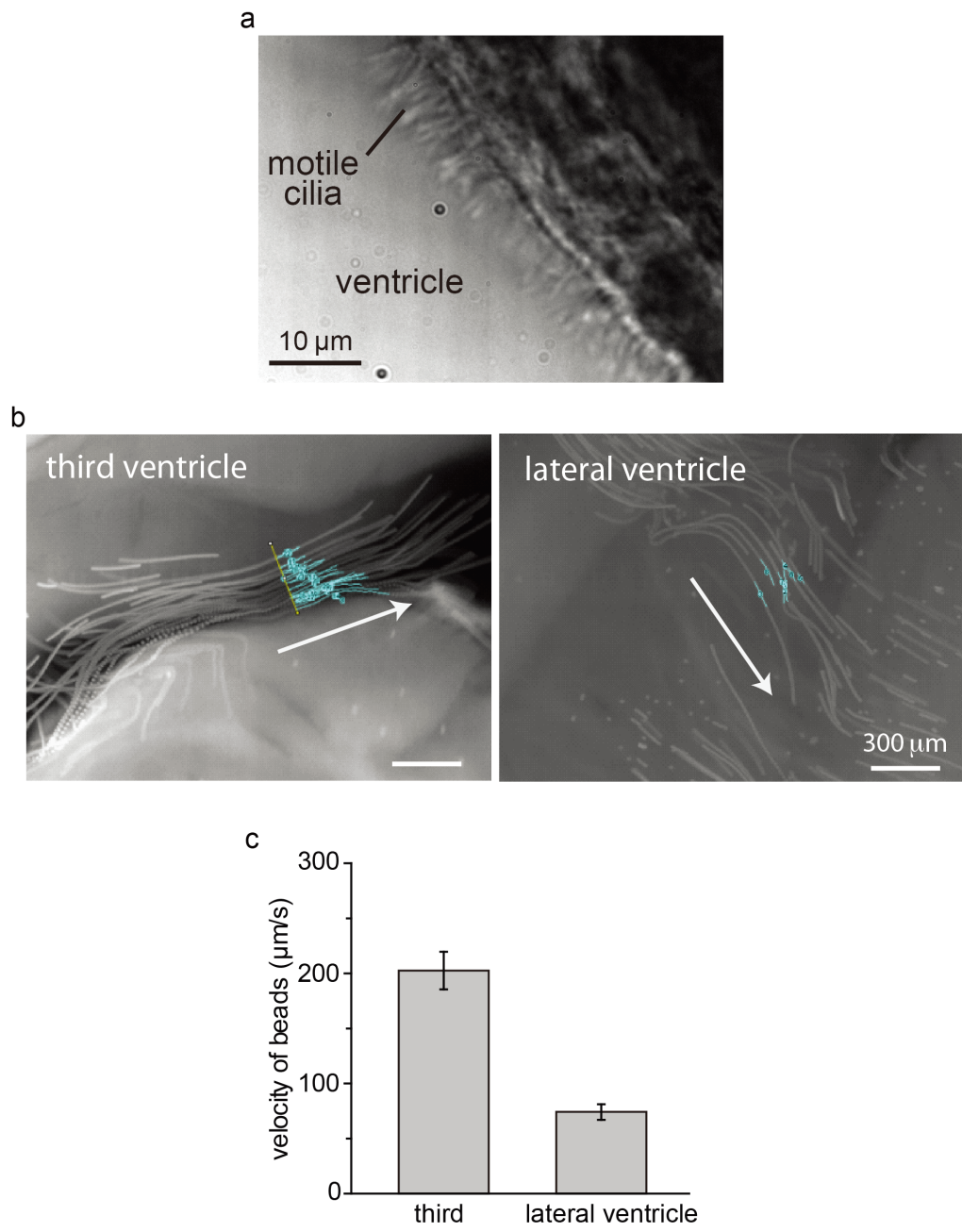


Figure S2

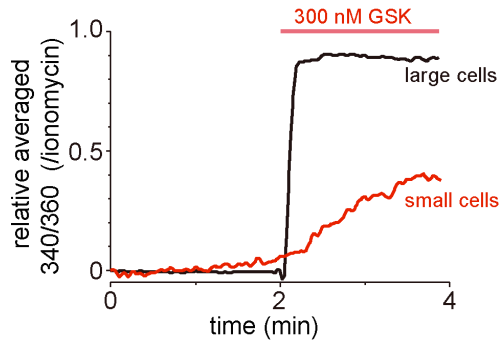


Figure S3

